HHS Public Access

Author manuscript

Cell Rep. Author manuscript; available in PMC 2024 December 23.

Published in final edited form as:

Cell Rep. 2024 November 26; 43(11): 114880. doi:10.1016/j.celrep.2024.114880.

Ventral hippocampal interneurons govern extinction and relapse of contextual associations

Anthony F. Lacagnina[1,2], **Tri N. Dong**[1,2], **Rasika R. Iyer**[1,2], **Leonie F. Boesch**[1,2], **Saqib Khan**[1,2], **Mazen K. Mohamed**[1,2], **Roger L. Clem**[1,2,3,*]

[1]Nash Family Department of Neuroscience, Icahn School of Medicine at Mount Sinai, New York, NY, USA

[2]Friedman Brain Institute, Icahn School of Medicine at Mount Sinai, New York, NY, USA

[3]Lead contact

SUMMARY

Contextual memories are critical for survival but must be extinguished when new conditions render them nonproductive. By most accounts, extinction forms a new memory that competes with the original association for control over behavior, but the underlying circuit mechanisms remain largely enigmatic. Here, we demonstrate that extinction of contextual fear conditioning recruits somatostatin interneurons (SST-INs) in the ventral hippocampus. Correspondingly, real-time activity of SST-INs correlates with transitions between immobility and movement, signaling exit from defensive freezing bouts. Optogenetic manipulation of SST-INs but not parvalbumin interneurons (PV-INs) elicits bidirectional changes in freezing that are specific to the context in which extinction was acquired. Finally, similar effects were obtained following extinction of sucrose-based appetitive conditioning, in which SST-IN inhibition triggers relapse to reward seeking. These data suggest that ventral hippocampal SST-INs play a fundamental role in extinction that is independent of affective valence and may be related to their disruption of spontaneous emotional responses.

In brief

Lacagnina et al. demonstrate that somatostatin interneurons in the ventral hippocampus control extinction of contextual associations. This establishes a general circuit mechanism for disengagement from conditioned emotional responses.

Graphical abstract

*Correspondence: roger.clem@mssm.edu.

AUTHOR CONTRIBUTIONS

A.F.L. and R.L.C. initiated the project. R.L.C. supervised the research. R.L.C., A.F.L., and T.N.D. designed experiments. A.F.L., T.N.D., R.R.I., L.F.B., S.K., and M.K.M. performed the research and analyzed the data. A.F.L. and R.L.C. wrote the manuscript.

DECLARATION OF INTERESTS

The authors declare no competing interests.

SUPPLEMENTAL INFORMATION

Supplemental information can be found online at https://doi.org/10.1016/j.celrep.2024.114880.

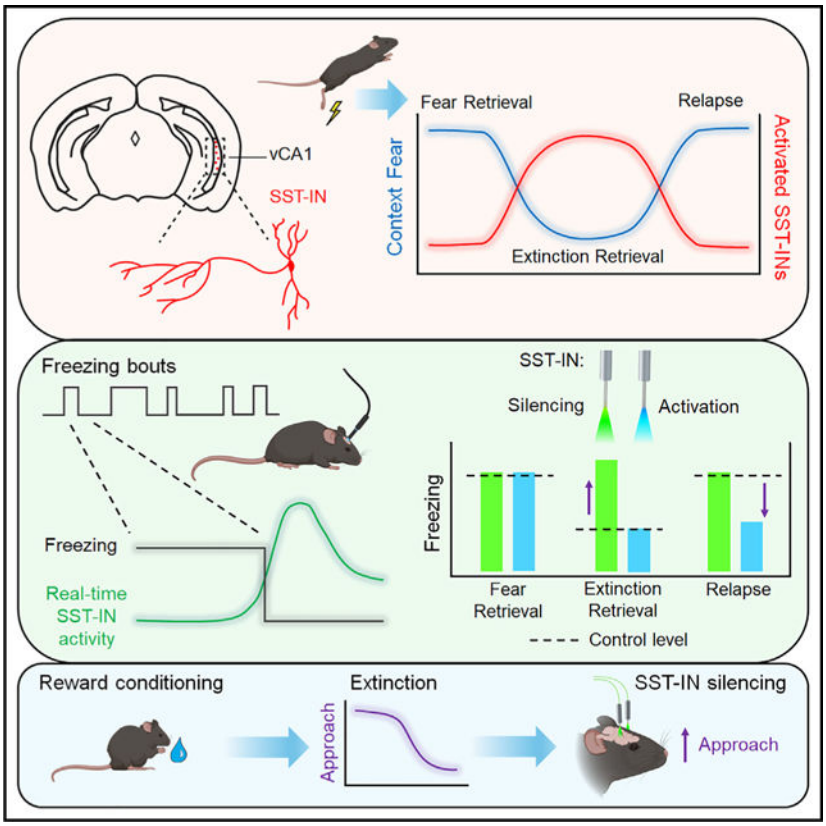

INTRODUCTION

Animals associate positive and negative events with configural representations of their environments to facilitate the expression of context-appropriate behaviors. However, when the environment changes, this learning may no longer be productive or can even become detrimental. Under this circumstance, extinction is a form of long-term memory that attenuates responding in the absence of positive or negative reinforcement.[1,2] Such behavioral flexibility plays a pivotal role in recovery from trauma and addiction, but its efficacy is limited by the tendency for extinguished behavioral responses to reemerge.[3–6] A potential solution to relapse might entail biasing expression of the extinction memory over previously learned associations.

Contextual learning is probably best understood in fear conditioning, which is thought to be acquired through experience-dependent synaptic plasticity and represented at the neural circuit level by an assembly of neurons.[7,8] Extinction attenuates behavioral and neural correlates of fear but does not abolish the original threat association, whose expression can be recovered by certain triggers.[9] A favored explanation has been that fear and extinction memories are stored alongside one another and compete for control over behavior,[10–16] but the mechanisms controlling their selection remain unclear. Indeed, while both forms of learning induce spatial remapping of hippocampal neurons,[17–20] an important unanswered question is whether neurons that gate extinction retrieval are functionally distinct in terms of their molecular or physiological properties from those involved in fear expression.

Furthermore, the implications for extinction under normal and pathological conditions will depend on whether such a mechanism is specific to threat-based behavior or generalizes to other forms of learning.

To answer these questions, we performed an immunohistochemical screen of brain regions involved in fear learning to identify areas exhibiting differential activity during successful extinction retrieval, as indicated by immunolabeling for the immediate-early gene c-Fos. Because somatostatin interneurons (SST-INs) throughout this network are implicated in acquisition and discrimination of fear-related stimuli,[21–28] we focused on any global differences in c-Fos labeling as well as those specific to SST-INs. We found that fear regulation was associated with contrasting patterns of activity in the prelimbic cortex (PL) and ventral CA1 region of the hippocampus (vCA1), where SST-INs were found to be selectively engaged by retrieval of either fear or extinction memory, respectively. In the vCA1, optogenetic manipulation of SST-INs elicited bidirectional changes in fear expression that were both context and learning specific and could not be mimicked by parvalbumin interneuron (PV-IN) stimulation. Similar recruitment of vCA1 SST-INs was observed following extinction of sucrose reward conditioning, and suppression of SST-INs evoked relapse of reward seeking. Our results suggest that extinction of contextual associations is controlled by a discrete form of GABAergic inhibition, which could be a general mechanism for disengaging from learned emotional responses.

RESULTS

Retrieval of contextual fear extinction preferentially activates vCA1 SST-INs

While expression of fear memory depends on activation of specific cell populations associated with a discrete cue or context, extinction is thought to form a competing association that signals safety in the presence of previously threatening stimuli. Accordingly, successful recall of extinction recruits sparse neuronal populations whose reactivation contributes to low fear expression.[12–14,16] Less understood is whether distinct circuit elements (e.g., neurons with unique molecular or anatomical features) might facilitate extinction memory or promote its expression over conditioned fear. To begin addressing this question, we used c-Fos immunohistochemistry to identify brain regions preferentially activated by extinction retrieval. In addition, given our prior work establishing an important causal role for SST-IN signaling in fear memory,[22,23] we specifically investigated whether activation of region-specific SST-IN populations differs in extinguished versus non-extinguished mice. The use of c-Fos as a proxy for SST-IN activation in these brain structures is supported by numerous reports, including those in which upregulation of c-Fos was confirmed following artificial activity manipulations.[22,23,26,27,29–31]

To model extinction retrieval, male and female SST-Cre::Ai9 transgenic mice were first submitted to contextual fear conditioning followed by extinction training entailing 5 daily exposures (10 min) to the conditioned context (Ext Ret group; Figure 1A). Another subset of animals received no extinction training and instead remained in their home cages (Fear Ret group). Additionally, to control for independent effects of repeated context exposure during extinction, a third group was treated identically to Ext Ret mice except that foot shocks were omitted during conditioning (No Shock group). On the final day, all mice were re-exposed

to the conditioned context and then sacrificed for immunohistochemical analysis of the prefrontal, hippocampal and amygdala subregions, which form a network highly implicated in fear memory.[32] Freezing during the final test was strongly attenuated in Ext Ret compared to Fear Ret mice and did not differ from No Shock controls (Figure 1B).

Among the regions analyzed, the PL exhibited a higher density of c-Fos$^+$ neurons as well as a higher density and proportion of c-Fos$^+$ SST-INs in Fear Ret mice relative to both remaining groups (Figures 1C and 1D), suggesting that, similar to prior observations following auditory fear conditioning, contextual fear recall engages prelimbic circuitry involving SST-INs, and this activation is reversed with extinction learning.[22,23] However, no differences were noted in either the total number of c-Fos$^+$ cells or c-Fos$^+$ SST-INs in the infralimbic cortex or lateral or basal amygdala (Figures S1A, S1C, and S1D). Likewise, a similar number of immunopositive cells was observed in the granule cell layer of the dentate gyrus and stratum pyramidale (s.p.) of areas CA1 and CA3 in both the dorsal and ventral hippocampus (Figures S1E, S1G, S1I, S1K, and S1M). However, c-Fos was elevated in Ext Ret mice within the vCA1 and, to a lesser extent, dorsal CA1 in the stratum oriens (s.o.) (Figures 1E, 1F, and S1J), which is populated primarily by GABAergic neurons and contains the majority of hippocampal SST-INs.[33] Moreover, a higher density and overall proportion of vCA1 SST-INs were found to be co-labeled for c-Fos in Ext Ret mice. Thus, recall of fear and extinction memory elicits contrasting patterns of activity in the prefrontal cortex and vCA1, respectively, and vCA1 SST-INs are preferentially activated following extinction. Extinction was also associated with a lower proportion of c-Fos$^+$ hilar SST-INs in the dorsal dentate gyrus (Figure S1F), but we concentrated our efforts in this study to understanding the functional role of vCA1 populations.

One possibility is that vCA1 SST-INs become engaged following extinction to facilitate the expression of newly adapted behavior (i.e., cessation of freezing). Alternatively, increased vCA1 SST-IN activity may reflect changes driven by extinction learning but not necessarily related to extinction retrieval. Notably, extinction learning is susceptible to relapse, in which expression of the original fear association returns despite successful extinction learning.[9] We therefore examined c-Fos expression under a relapse scenario to further test modulation of SST-IN activity by high- and low-fear states. As above, SST-Cre::Ai9 mice received contextual fear conditioning followed by extinction training (Figure 1G). One day later, they were returned to the conditioned context, where one group of mice received a single reminder shock (Reminder group). This condition is a well-established trigger of relapse, potentially mediated by relearning, reinstatement, or some combination thereof.[9] During a final test session, the Reminder group exhibited higher freezing levels in the conditioned context compared to animals for which the reminder shock was omitted (No Reminder group; Figure 1H). Correspondingly, animals receiving the reminder shock displayed fewer c-Fos$^+$ cells in the s.o. as well as c-Fos$^+$ SST-INs in the vCA1 (Figure 1I). This further indicates that SST-IN activation is associated with low fear expression and subject to opposing modulation by extinction and relapse.

During our analysis, we noted that, similar to other recent studies,[34,35] SST-Cre::Ai9 mice exhibit conditional expression of tdTomato in a subset of neurons in the s.p. with pyramidal morphology in the vCA1 and vCA3 (Figure S2A). Immunolabeling revealed

that the vast majority of tdTomato$^+$ cells in the s.o. but not the s.p. express somatostatin (Figures S2E–S2G). However, to determine whether more selective targeting of SST-INs can be achieved, we compared these results to those from SST-FlpO::Ai65f mice, in which reporter expression relies on Flp rather than Cre recombination. As in the SST-Cre line, SST-FlpO::Ai65f mice exhibited a similar abundance of tdTomato expression in the s.o., and tdTomato$^+$ cells were predominantly immunopositive for SST. However, in contrast to SST-Cre::Ai9 mice, SST-FlpO::Ai65f mice were relatively lacking in pyramidal cell labeling (Figure S2). We therefore selected the SST-FlpO line for subsequent *in vivo* manipulations of SST-INs to minimize potential off-target effects.

Extinction is associated with alterations in SST-IN synaptic drive, but these are not attributable to plasticity of SST-IN synapses

Prior reports indicate that SST-INs in the dorsal CA1 (dCA1) express long-term potentiation at excitatory synapses and exhibit experience-dependent plasticity following contextual fear conditioning.[21,36]We therefore wondered whether vCA1SST-INs might, at a more remote time point after conditioning, exhibit either fear or extinction-related alterations in synaptic transmission. SST-Cre::Ai9 mice were subjected to fear conditioning with or without subsequent extinction using the same behavioral design as shown in Figure 1, except a final test of memory retrieval was omitted, and instead we prepared transverse acute slices of the vCA1 (Figure 2A). Importantly, extinction yielded a reduction in freezing across training sessions (Extinction group; Figure S3). SST-INs were targeted for whole-cell recordings based on s.o. location and tdTomato expression, and the properties of both spontaneous excitatory postsynaptic currents (sEPSCs) and inhibitory postsynaptic currents (sIPSCs) were analyzed.

The results indicated that SST-INs from extinguished mice exhibited a higher frequency of sEPSCs relative to non-extinguished mice (Extinction vs. Fear Cond; Figures 2B–2D). However, neither group differed from No Shock controls. Conversely, extinction was associated with lower amplitude of sIPSCs relative to No Shock controls as well as a statistical trend toward lower amplitude relative to Fear Cond mice (Figures 2B and 2E). Given these mixed effects, we examined whether there were any differences in the balance of excitatory:inhibitory transmission (E:I ratio) at the level of individual SST-INs, relying on a charge-based metric that accounts for both frequency and amplitude of currents (Figure 2F). This analysis revealed that, compared to SST-INs from Fear Cond mice, SST-INs from Extinction mice exhibited a higher E:I ratio of spontaneous transmission. However, when this experiment was repeated in the presence of tetrodotoxin (TTX; 1 μM), no group differences in these metrics were observed (Figures 2C and 2G–2I), indicating that the increased E:I ratio was not attributable to plasticity of SST-INs but may instead result from changes in network excitability (e.g., increased firing of presynaptic cell populations).

Real-time SST-IN activity is organized around defensive freezing bouts and modulated by extinction

To gain insight into the *in vivo* response properties of vCA1 SST-INs, we used fiber photometry to monitor their activity during acquisition, extinction, and relapse of contextual fear conditioning (Figures 3A–3C). In addition, to establish context specificity of any

effects, imaging was repeated in an arena distinct from the one where conditioning and extinction occurred (Alt Ctx). Prior to these behavioral assays, SST-FlpO mice received hippocampal infusions of AAV-fDIO-GCaMP6s and were implanted with optic fibers directed at the vCA1 (Figures 3A and 3B). As expected, subjects exhibited bidirectional modulation of percentage time freezing during conditioning, extinction, and relapse tests (Figure 3D). Decreased freezing during extinction corresponded primarily to a reduction in the duration but not the frequency of freezing bouts, an effect that was reversed during subsequent relapse (Figures S4A–S4E). Analysis of spontaneous Ca^{2+}-related transients revealed an increase in their amplitude during extinction session 5 compared to a pre-training baseline (Figures 3E and 3F). This increase was specific to the conditioning arena and not observed in an alternate context where the animal had received no shocks. Examination of Ca^{2+} event frequency also revealed a slight increase in interevent interval in the relapse test relative to extinction session 1 (Figure 3G).

Alignment of Ca^{2+} signals to behavioral events revealed that SST-INs exhibit prominent excitatory responses to foot shock and that these exhibit a trial-dependent increase in magnitude across fear conditioning (Figures S4F–S4I). In addition, onset and offset of individual freezing bouts were associated with decreased and increased in SST-IN activity, respectively (Figures 3H–3K). This modulation was evident as early as conditioning, when freezing was first observed, but offset responses increased considerably in magnitude during extinction and relapse sessions. While subsequent exposure to an alternate context also elicited a low level of freezing, with characteristics similar to the final extinction session (Figures 3D and S4), individual freezing bouts in the alternate context were correlated with smaller offset responses in SST-INs. Collectively, these data indicate that SST-IN activity is inversely correlated with freezing and may recalibrate fear expression in an experience-dependent manner; for example, by promoting exit from defensive freezing bouts. SST-INs become more responsive to freezing transitions during extinction, and this pattern is selectively enhanced in the conditioning context relative to a distinct arena where animals express a low level of generalized freezing, suggesting a role for SST-INs in context-specific adaptation.

SST-INs control context-evoked freezing after extinction

To test whether vCA1 SST-INs indeed regulate fear expression, we turned to an optogenetic approach in SST-FlpO mice, using a within-animal behavioral design in which halorhodopsin (NpHR)-mediated photoinhibition or channelrhodopsin (ChR2)-mediated photoexcitation was conducted at key time points following acquisition, extinction, and relapse of contextual fear conditioning (Figures 4A–4C and S5). In addition, to establish context specificity of any effects, photostimulation was repeated in an arena distinct from the one where conditioning occurred. Finally, for each manipulation, an opsin-negative control vector (eYFP only) was infused into a separate group of animals to control for independent effects of laser light.

Prior work indicates that freezing is typically strongest during the initial few minutes of exposure to a conditioned context.[13] We therefore targeted the initial 3-min epoch of each 12-min test for photostimulation, with the rationale that our manipulations would be most

likely to influence behavior at this stage. However, a second period of photostimulation was also included to examine the impact of SST-IN activity later in each test session. Analysis of light-on (532 nm, 12–15 mW, constant) and light-off epochs across all tests in NpHR and eYFP mice revealed an opsin 3 epoch interaction, which could be attributed to higher freezing in NpHR relative to eYFP mice during the extinction retrieval test (Figure 4D). This effect was specific to the first epoch of the extinction retrieval test, mirroring a prior study involving dentate granule cell inactivation,[13] and did not occur during photoinhibition in an alternate context (Figure 4D). Further analysis of within-animal freezing (restricted to the initial 3-min epoch) confirmed that NpHR but not eYFP mice exhibited relapse of freezing between the final extinction session and the subsequent extinction retrieval test (Figure 4E).

We next conducted a similar analysis of behavior during SST-IN photoexcitation (473 nm, 9–12 mW, 20 Hz, 10 ms pulses), which revealed an opsin × epoch interaction across test sessions, as well as lower freezing in ChR2 relative to eYFP mice during the first epoch of the relapse test (Figure 4F). Further analysis of within-animal freezing confirmed that, while eYFP mice exhibited relapse after a reminder shock, this effect was abolished in ChR2 mice (Figure 4G). However, photoexcitation did not attenuate freezing during the initial test of fear retrieval (Figure 4F), suggesting that extinction learning was required before SST-INs could exert control over fear expression. Furthermore, there was no effect of photoexcitation in an alternate context, indicating that SST-IN activation did not interfere generally with contextual discrimination processes, leading to fear generalization. Finally, neither NpHR nor ChR2 mice exhibited general locomotor effects upon photostimulation in the open field assay (Figures S5B and S5D). Thus, vCA1 SST-INs modulate fear under specific scenarios when memories of threat and safety are in conflict. In these situations, SST-IN activity is important for extinction recall and attenuates freezing.

Control of context fear extinction is a function of specific interneurons

While activating SST-INs reduces freezing under relapse conditions, it is nevertheless possible that stimulation of any large inhibitory population has the potential to disrupt in a broad or nonselective manner the function of vCA1 neurons and may not be indicative of the specific functional capacity of extinction-related SST-INs. Therefore, we first asked whether relapse of extinguished fear can be prevented by reactivating SST-INs that were specifically recruited by extinction learning. For this purpose, we employed a viral genetic strategy entailing expression of an estrogen receptor-dependent Cre recombinase (ERCreER) under the control of the enhanced synaptic activity responsive element (E-SARE) (Figures 5A and 5B).[37] In a prior report, we demonstrated that this approach effectively labels memory-related SST-INs when used in combination with SST-FlpO driver mice for intersectional recombination.[22] To determine whether E-SARE is suitable for tagging extinction-related SST-INs, we infused AAV-E-SARE-ERCreER into the vCA1 along with an intronic recombinase sites enabling combinatorial targeting (INTRSECT) eYFP vector, which requires both Cre and Flp recombination for eYFP transcription (Figure 5B). Subjects were then divided into two groups, both of which underwent contextual fear conditioning and extinction but received injections of 4-hydroxytamoxifen (4-OHT) at different time points to compare resulting cellular tagging (Figure 5C). Consistent with c-Fos analysis (Figure 1F), mice that received 4-OHT during the final extinction session exhibited more abundant

labeling within the vCA1 s.o. than those injected following fear conditioning (Figures 5D and 5E). However, labeling within the s.p. was exceedingly sparse and not modulated by timing of injection (Figure 5E), consistent with preferential targeting of SST-INs.

Using the above intersectional genetic strategy, we next targeted extinction-related SST-INs for cellular tagging with either ChR2 or eYFP (Figure 5F). Following infusion of E-SARE and INTRSECT constructs into the vCA1, all subjects underwent fear conditioning and extinction and were injected following the final extinction session with 4-OHT to induce recombination in extinction-related SST-INs (Figure 5G). Following viral expression, effects of photoexcitation on conditioned freezing were tested during extinction retrieval, relapse, and alternate context exposure. Analysis of light-on and light-off epochs across all tests revealed an opsin 3 epoch interaction. As with bulk excitation of SST-INs (Figure 4E), ChR2-expressing mice exhibited lower freezing than eYFP mice during the relapse test (Figure 5I), which was attributable to a lack of fear return in this group following a reminder shock. No differences were observed during the other context tests or during free exploration of the open field (Figures 5I and S5F). Therefore, reactivation of a sparse population of extinction-related interneurons is sufficient to attenuate freezing despite their comprising a minority (~25%) of vCA1 SST-INs.

Nevertheless, while targeting a subset of memory-related SST-INs can avoid potentially nonselective effects, it is nevertheless unclear whether the capacity to inhibit freezing is unique to SST-INs, which are distinct in terms of morphology and synaptic connectivity from other interneuron classes. PV-INs represent the largest subclass of interneurons in the vCA1 aside from SST-INs and exert profound control over the firing of excitatory projection neurons.[38] We therefore tested whether extinction-related behavior could be modulated by photoexcitation of PV-INs using a design identical to that employed for SST-IN manipulations (Figure 6C). In these experiments, PV-Cre mice were employed to restrict expression of Cre-dependent ChR2 or eYFP vectors to PV-INs (Figures 6A and 6B). Unlike manipulations of SST-INs, our analysis revealed no effect of opsin expression in these experiments despite successful acquisition of extinction by both ChR2 and eYFP groups (Figure S5G). Furthermore, both ChR2 and eYFP groups exhibited return of freezing following a reminder shock (Figure 6D), indicating that PV-IN activation failed to prevent relapse. Thus, fear-attenuating effects of SST-INs cannot be mimicked by another source of inhibition and are therefore likely to depend on discrete microcircuit dynamics rather than non-selective impairments in hippocampal processing.

SST-INs also mediate extinction of appetitive contextual associations

The pattern of results obtained following contextual fear conditioning are intriguing in that SST-IN manipulations affected specific stages of behavior. We found no evidence that SST-INs gate freezing prior to extinction learning or in a distinct context where learning did not occur, suggesting that involvement of SST-INs in modulating these responses cannot be explained in terms of a general role in aversive behavior. Therefore, to test whether SST-INs support extinction under non-aversive conditions, we implemented a form of Pavlovian contexual appetitive conditioning in which learning is indicated by approach to a reward delivery port. First, adopting a design similar to that used for c-Fos analysis after

fear extinction (Figure 1), we tested whether extinction of contextual reward conditioning activates SST-INs. SST-Cre::Ai9 mice were deprived to 80%–90% of free-feeding weight and divided into three groups that were continuously rewarded throughout 14 days of training (Reward Ret), rewarded only on the first 8 days (Ext Ret), or repeatedly exposed to the conditioning context without ever receiving sucrose within the context (No Reward) (Figure 7A). The Reward Ret and Ext Ret groups exhibited increased port entries across training sessions until day 9, after which responding remained high in the Reward Ret condition but was strongly attenuated in Ext Ret mice (Figure 7B). Following extinction, all groups were returned to the conditioning context, and their behavior was examined in the absence of any sucrose delivery before they were sacrificed for immunohistochemical analysis.

Compared to the Reward Ret group, Ext Ret mice made fewer port entries during the final test, and their performance was equivalent to the No Reward group (Figure 7C). Examination of prefrontal brain sections revealed a greater density of c-Fos$^+$ cells in the prelimbic region of Reward Ret compared to No Reward mice (Figure S6), mirroring group differences observed following contextual fear conditioning (Figure 1). Likewise, Ext Ret mice exhibited a higher density of c-Fos labeling in the vCA1 s.o. and a higher proportion of c-Fos$^+$ SST-INs (Figures 7D and 7E).

Given these results, we tested whether SST-IN activity influences recall of sucrose reward extinction. SST-FlpO mice received vCA1 injections of Flp-dependent NpHR or eYFP vectors and, following a period of incubation, were submitted to contextual reward conditioning and extinction (Figures 7F–7H). Both groups exhibited increased port entries as a function of training and an equivalent reduction in responding during extinction (Figure 7H). Following extinction, animals were returned to the reward context, and the behavioral effect of photoinhibition was tested in the absence of reward. During this test, NpHR-expressing mice made a greater number of port entries than eYFP mice, consistent with relapse of an extinguished reward association (Figure 7I). These results indicate that SST-INs gate extinction retrieval independent of the affective valence of conditioning or whether learning is expressed through an active or passive response.

DISCUSSION

In this study, we uncovered neural activity patterns linked to contextual fear extinction and established a specific functional role for ventral hippocampal SST-INs in extinction retrieval.

After extinction, SST-INs in the vCA1 exhibit heightened activation in response to exposure to the extinguished context, and their activity is highly organized around defensive freezing bouts. Paralleling extinction-dependent engagement of SST-INs, effects of manipulating this population are highly selective to the context where extinction learning occurred and do not affect initial fear expression. This implies that vCA1 SST-INs are not hardwired to control aversive behavior but, rather, modulate expression of conflicting fear and extinction memories in an experience-dependent manner. Accordingly, our examination of reward-based learning revealed a similar pattern of results, and despite its culmination in an

active behavioral output (i.e., approach), we found a shared requirement for SST-INs in the expression of appetitive extinction memory.

In freely behaving mice, an inverse relationship between SST-IN activity and conditioned fear expression was evident even over short timescales, with SST-INs signaling exit from individual freezing bouts. With the return of high freezing levels after relapse, we therefore expected to find reduced SST-IN activity, a prediction that was confirmed by c-Fos immunolabeling but not by fiber photometry analysis. However, these methods differ in their sensitivity to activity as well as their ability to resolve specific neurons. Therefore, it is possible that c-Fos delineates a subset of SST-INs defined by a specific rate or pattern of activity that is important for extinction. Another unresolved question is why freezing was attenuated by SST-IN photoexcitation following extinction and relapse but not at an earlier time point after fear conditioning. Perhaps a gain in functional capacity of SST-INs can be explained by changes in how vCA1 neurons respond to GABAergic inhibition or how vCA1 output is integrated by downstream brain regions.

The circuit mechanism by which vCA1 SST-INs ultimately influence memory processing remains unclear but is likely to depend on their interaction with local excitatory projection neurons. In support of this possibility, a recent report indicates that putative projection neurons in the vCA1 exhibit increased activity during freezing,[39] a pattern complementary to that of SST-INs. This could imply that fear expression relies on reactivation of excitatory ensembles under inhibitory control of extinction-related SST-INs. If true, then this is unlikely to result from general network inhibition because we did not observe differences in cFos labeling of the pyramidal cell layer after extinction (Figure S1B), and behavioral relapse could not be prevented by stimulation of a different inhibitory population (PV-INs; Figure 6). Instead, our results suggest that the unique synaptic configuration of SST-INs may be as important as their inhibitory output, in which case SST-IN microcircuits exhibit several unique properties that may warrant consideration. First, a large proportion of SST-INs in the CA1 preferentially innervate the distal dendritic compartment of pyramidal neurons, where they influence the integration of direct entorhinal inputs.[40,41] Interestingly, layer III neurons of the medial entorhinal cortex, which give rise to these inputs, play an instructive role in reward-based spatial remapping and drive dendritic plateau potentials near reward locations.[42] It is possible that fear conditioning relies on an analogous dendritic signal and that its disruption by SST-IN-mediated inhibition prevents reactivation of a fear-related assembly or exerts feedback control on these cellular dynamics.

Aside from excitatory neurons, SST-INs also synapse extensively onto other interneuron subtypes, including PV-INs and Schaffer collateral-associated interneurons (SC-INs), for which cholecystokinin is a specific marker.[43–45] By interacting with these populations, SST-INs could influence network dynamics through disinhibition to support the recruitment of new cellular assemblies established by extinction learning. While our data appear to exclude PV-INs as potential mediators of such effects, SC-INs are an important source of feedforward inhibition in the SC pathway, where interaction between SST-INs and SC-INs facilitates synaptic integration of CA3 inputs by CA1 pyramidal cells.[40] Thus, signaling from both major afferent pathways controlling CA1 activity can be shaped by SST-INs, potentially in a coordinated fashion that favors processing of some inputs (i.e., CA3) over

others (i.e., entorhinal). As the dentate gyrus and CA3 are thought to perform a pattern separation and completion transformation,[46] vCA1 SST-INs may play a role in gating information arriving from CA3 in order to disambiguate conflicting memories associated with the context. In addition to pathway-specific control, however, SST-INs support type II theta oscillations, which may contribute to the expression of prior learning through entrainment of discrete ensembles across hippocampal-prefrontal networks.[47,48]

Just as the downstream effects of SST-IN activity remain to be established, another important question is by what mechanism are they activated in extinction retrieval. Because SST-INs derive a large proportion of their input from local excitatory neurons,[33] it seems plausible that dynamic changes in vCA1 population activity are responsible for their recruitment. In this scenario, SST-INs may participate as a component of an extinction-related assembly whose function is to resolve a conflict between new and prior learning through feedback control of competing populations.[26] Alternatively, inputs originating outside the hippocampus may be more critical in orchestrating SST-IN activity. For example, SST-INs exhibit potent activation in response to cholinergic signaling,[24,41,49,50] which may explain a selective requirement for the medial septum in extinction but not acquisition of contextual fear.[19]

Regardless of the underlying circuit mechanisms, an intriguing facet to our results is that SST-INs exert similar control over aversive and appetitive associations. Recent work on olfactory-based conditioning suggests that, in contrast to the dCA1, the vCA1 preferentially encodes stimuli with emotional significance, and once formed, these representations are relatively stable when the conditioned stimulus is paired with an outcome of opposite affective valence.[51] This has been interpreted to mean that, while vCA1 populations multiplex information about stimulus outcomes, they may also track the current value or salience of a stimulus independent of its associative valence. Future work will be needed to resolve the role of distinct efferent pathways of the vCA1 in controlling valence-specific action and whether projections that signal stimulus salience and/or outcome are preferentially modulated by SST-INs.

To conclude, our results suggest that SST-INs are an important substrate for contextual fear extinction that may hold clues about the flexible representation of both aversive and appetitive experiences. When activated, SST-INs function like a mnemonic gate that controls whether new or old learning prevails. As such, they can override established stimulus responses to allow animals to engage in competing adaptive behaviors and potentially encode new stimulus relationships.

Limitations of the study

Our findings suggest that there are a greater number of activated SST-INs in the vCA1 following fear extinction and that these neurons may increase their firing in conjunction with termination of freezing. However, bulk calcium imaging does not provide direct confirmation of this possibility, and c-Fos labeling cannot be directly related to event-related photometry signals. Activity monitoring at cellular resolution would provide more insight into the response patterns of individual SST-INs and how they are modified in conjunction with behavioral responses. Another important limitation of this study is that it does not

address the functional role of SST-INs more broadly in various forms of relapse, which can occur in response to stress, internal state changes, or even the mere passage of time. Whether these situations engage a common circuit mechanism to promote the return of conditioned emotional responses remains unclear. Therefore, it is possible that different relapse states might vary in their sensitivity to vCA1 SST-IN manipulations.

RESOURCE AVAILABILITY

Lead contact

Requests for further information, resources, and reagents should be directed to and will be fulfilled by the lead contact, Roger L. Clem (roger.clem@mssm.edu).

Materials availability

This study did not generate new unique reagents or mouse lines.

Data and code availability

- Data are available in the figures and from the lead contact.
- This paper does not report original code.
- Any additional information required to reanalyze the data reported in this work is available from the lead contact upon request.

STAR★METHODS

EXPERIMENTAL MODEL AND STUDY PARTICIPANT DETAILS

Adult male and female mice aged 2–6 months were used in all experiments. All transgenic mice were originally acquired from The Jackson Laboratory and were subsequently bred in-house. Mice were housed in groups of 2–5 in plastic cages with corncob bedding and cotton nestlets and were maintained on a 12 h light-dark cycle (7:00–19:00) in a temperature- and humidity-controlled vivarium. Food and water were provided ad *libitium*, except for appetitive conditioning experiments where food was restricted. All experiments were performed during the light cycle. Mice were randomly assigned to groups prior to experimentation. Sample sizes were chosen to meet or exceed those used in previously published studies using similar experimental designs. The following transgenic mouse lines were used: SST-Cre (stock number 028864; B6J.Cg-*Sst*$^{tm2.1(cre)Zjh}$/MwarJ), SST-FlpO (stock number 028579; *Sst*$^{tm3.1(flpo)Zjh}$/J), Ai9 (stock number 007909, B6.Cg-*Gt(ROSA)26Sor*$^{tm9(CAG-tdTomato)Hze}$/J) mice, Ai65f (stock number 032864; B6.Cg-*Gt(ROSA) 26Sor*$^{tm65.2(CAG-tdTomato)Hze}$/J), and PV-Cre (stock number 017320; B6.129P2-*Pvalb*$^{tm1(cre)Arbr}$/J). All experimental procedures were approved by the Institutional Animal Care and Use Committee at the Icahn School of Medicine at Mount Sinai.

METHOD DETAILS

Viral vectors—Viral vectors purchased from Addgene include AAV1-Ef1a-fDIO-eYFP (#55641), AAV8-nEF-Coff/Fon-ChR2(ET/TC)-eYFP (#137141), AAV8-nEF-Coff/Fon-NpHR3.3-eYFP (#137154), AAV8-hSyn-Con/Fon-eYFP (#55650), AAV8-hSyn-Con/Fon

hChR2(H134R)-eYFP (#55645), AAV8-Ef1a-fDIO-GCaMP6s (#105714) and AAV1-Ef1a-DIO-hChR2(H134R)-eYFP (#20298). The plasmid for E-SARE-ERCreER-PEST was obtained as a gift from Dr. H. Bito (University of Tokyo), then expanded in transformation-competent *E. coli* and purified with a Qiagen MaxiPrep kit, followed by extraction in a solution of phenol-chloroform-isoamyl alcohol (25:24:1) saturated with 10 mM Tris (pH 8.0) and 1 mM ethylenediaminetetraacetic acid (EDTA). The purified plasmid was packaged in an AAV8 serotype at the Boston Children's Hospital vector core. For intersectional activity-dependent tagging, vectors were mixed in a 1:4 ratio of E-SARE-ERCreER to Cre_{on}/Flp_{on}-ChR2-eYFP or Cre_{on}/Flp_{on}-eYFP, respectively. Following expression, clearance of ERCreER is enhanced by PEST-mediated degradation to ensure a brief temporal window for cellular tagging.[37]

Optic fiber construction—Fiber optic implants used in optogenetic experiments were constructed using ceramic ferrules (1.25 mm outer diameter; Thorlabs) with a 200 μm core, 0.39 numerical aperture multimodal fiber (Thorlabs). Fibers were cut to 4 mm length to target vCA1 and polished through a series of decreasing grit aluminum oxide polishing papers (Thorlabs). Fiber efficiency was measured with a light intensity meter (Thorlabs) used for calibrating light intensity during behavioral manipulations.

Stereotaxic surgery—Stereotaxic viral infusion and optic fiber implantation surgery occurred 2–3 weeks before behavioral experimentation. Mice were anesthetized with vaporized 4% isofluorane in oxygen at 1.5 L min^{-1}, head-fixed in a stereotaxic surgical frame (Stoelting), and maintained under anesthesia of 1–1.5% at 0.75 L min^{-1}. Ophthalmic ointment was applied to the eyes to prevent drying. A skin incision was made to expose the skull. The skull was cleaned with 3% hydrogen peroxide and scored with a scalpel, and a craniotomy was drilled above the injection and fiber implant sites. Viral vectors were injected at a rate of 100 nL min^{-1} using a motorized injector (World Precision Instruments) and glass syringe (Hamilton). The needle was left in the injection site for an additional 5 min after infusion before being slowly retracted. For optogenetic experiments, viruses were infused bilaterally into vCA1 (from bregma; anteroposterior (AP): −3.16 mm; mediolateral (ML): ±3.5 mm; dorsoventral (DV): −3.5 and −4.1 mm) at a volume of 250 nL per injection site and fiber optic cannulas were implanted above the injection sites (AP: −3.16 mm; ML: ±3.5 mm; DV: −3.5 mm). For fiber photometry, mice received a unilateral viral infusion targeting vCA1 (350nL; AP: −3.16mm; ML: ±3.5 mm; DV: −3.75 mm) and an optic fiber (400 μm core; 0.48 numerical aperture; 2.5 mm metal ferrule; 4 mm length; Doric Lenses) was implanted above the injection site (AP: −3.16mm; ML: ±3.6 mm; DV: −3.6 mm). Implants were secured to the skull using C&B Metabond cement (Parkell) and dental cement (Lang). Mice were injected subcutaneously with banamine (2.5 mg kg^{-1} body weight) diluted in sterile saline (0.9%) to provide post-operative analgesia.

Contextual fear conditioning—All mice were handled for 1–2 min daily for 3–4 days before behavioral testing. For optogenetic and fiber photometry experiments, mice were then habituated to patch cords by allowing them to explore a novel cage while tethered to patch cables for 5 min. Mice were transported in their homecage from the vivarium to the holding room adjacent to the testing room at least 1 h prior to experimentation. For experimental

timelines involving optogenetic manipulation, mice were tethered to patch cables for all behavioral sessions regardless of whether laser light was delivered.

Behavioral testing was conducted in 30.5 (length) × 24 (width) × 21 (height) cm^3 conditioning chambers (Med Associates) with aluminum side walls, a Plexiglass door and ceiling, and a vinyl back wall. Conditioning chambers were housed within a larger sound-attenuating chamber. An overhead light and fan delivering ~65 dB ambient noise were present throughout every session. Two distinct contexts with unique sensory features were used – a conditioning context and alternate context. The conditioning context consisted of a stainless steel rod floor (36 rods spaced 8 mm apart measured center to center), and was cleaned and scented with 70% ethanol. The alternate context contained a curved plastic wall insert, a plastic floor covered with corncob bedding, and was cleaned and scented with isopropanol.

Contextual fear conditioning consisted of three 2 s 0.75 mA scrambled foot shocks delivered 180, 240, and 300 s after the start of the session. The mice were removed from the context 30 s after the last shock. Foot shocks were omitted for unconditioned mice. Baseline freezing is defined as the average freezing behavior during the first 3 min pre-shock period of this session.

Extinction training typically consisted of 5 daily sessions of 10 min unreinforced exposure to the conditioning context (exception: 5 min sessions for Figure 2). The average freezing behavior from the first 3 min of each extinction session is reported, as context-evoked freezing is typically highest during this period.[52] Mice that were not extinguished remained in their home cage until the test session.

The reminder shock session consisted of a single 2 s 0.75 mA shock delivered 180 s after the start of the session in the conditioning context, and mice were removed 30 s later. Average freezing from the 3 min pre-shock period was reported as the ‘pre-reminder’ period.

The final test sessions prior to perfusion for c-Fos analysis consisted of 5 min exposure to the conditioned context.

All behavioral sessions were recorded at 30 frames per second using a near-infrared camera mounted to the interior door of the sound-attenuating chamber and VideoFreeze software (Med Associates). The videos were manually scored for freezing behavior by an investigator blind to the experimental conditions. Freezing was defined as the absence of movement, with the exception of respiratory-related movements.

Fiber photometry imaging—Ca^{2+} fluorescence signals were recorded continuously throughout behavioral testing. Mice were connected via their implanted fiber optic ferrule to an imaging patch cord (400 μm core; 0.48 numerical aperture; Doric Lenses), which was coupled to a Fluorescence Mini Cube (Doric Lenses). Two LEDs (Doric Lenses) passed light through this patch cord at 465 nm to record the GCaMP6s-mediated SST-IN activity and at 405 nm as an isosbestic signal to control for motion artifacts and autofluorescence. Light intensity was set to 40 μW and was held constant across behavioral sessions. The LEDs were sinusoidally modulated at different frequencies to separate each

signal. Emitted light was collected through the same patch cord, passed through a dichroic mirror and emission filters, and was focused onto a photodetector (Model 2151 Femtowatt Photoreceiver, Newport). Signals were recorded and with a RZ5P real-time processor and Synapse software (v.90, Tucker-Davis Technologies), collected at a sampling frequency of 1017 Hz.

Fiber photometry analysis—Fiber photometry data were analyzed using the open-source, MATLAB-based pMAT software v.1.2.[53] Briefly, the Ca^{2+}-dependent signal (465 nm) and isosbestic control (405 nm) data are extracted and individually smoothed using a Lowess, local linear regression method. Next, the channels are normalized using a least-squares regression. The change in fluorescence (ΔF/F) was calculated by subtracting the normalized control channel from the Ca^{2+} signal. The fiber photometry and behavioral data were synchronized with a transistor-transistor logic (TTL) signal linked to the beginning and end of the behavioral session using a DC to TTL adapter (Med Associates) connected to the RZ5P processor.

For analysis of spontaneous Ca^{2+}-related events, the signal for the entire recording session was detrended using a polynomial function to remove gradual effects of photobleaching. The median absolute deviation of the resulting trace was calculated and the event threshold was set to two times this value. Local maxima exceeding the amplitude threshold were detected using Easy Electrophysiology (v2.6.3). Average amplitude (ΔF/F) and interevent interval were calculated and reported for the entire session. For the training session, transients resulting from foot shock were excluded.

Peri-event time histogram (PETH) analyses of behaviorally-aligned responses to freezing onset and offset were performed from −2 s to +2 s of the event and −5 s to +5 s for shock-elicited responses. A baseline sampling window was set as 5 s preceding the event for 5 s duration with a bin constant of 100 ms. Freezing bouts included in PETH analyses were filtered to only include bouts ≥1 s in duration and with ≥1 s of non-freezing behavior preceding a freezing onset event or following a freezing offset event to exclude events that were either too brief or overlapping with adjacent onset and offset periods. Average trace ΔF/F responses for behavioral events from each animal were exported to Prism v.10.2.3 (GraphPad) to calculate mean ΔF/F responses, AUC, and peak values.

Optogenetic manipulations during context tests—All optogenetic manipulation during context tests (fear retrieval, extinction retrieval, relapse, and alternate context) were 12 min in duration with light-on epochs occurring from min 0–3 and 6–9. NpHR-mediated photoinhibition was performed with a 568 nm laser (Opto Engine) delivered continuously with an intensity of 12–15 mW at the end of the fiber optic implant. ChR2-mediated photoexcitation was performed with a 473 nm laser (Opto Engine) delivered in 10ms pulses at 20 Hz with an intensity of 9–12 mW at the end of the fiber optic implant. All manipulations were performed bilaterally.

Open field test—The apparatus was a 40 (length) × 40 (width) × 30.5 (height) cm^3 box made of acrylic plastic with opaque walls. Overhead lights illuminated the center to ~200 lux. Mice were connected to fiber optic patch cables and placed into the arena for 18 min

and allowed to explore freely. Photostimulation consisted of 3 min light-on epochs from min 3–6, 9–12, and 15–18. The light parameters were identical to those used in contextual fear tests. The center zone was defined as an 18.5 × 18.5 cm^2 zone in the center of the arena. Movement was recorded using a digital camera mounted above the arena at 15 frames per second and was analyzed with Any-maze v. 6.33 video-tracking software (Stoelting).

Appetitive conditioning—All mice were food restricted to 80–90% of free-feeding weight beginning 5 days before behavioral testing and were weighed daily to maintain this deficit throughout the experiment. Mice were exposed to the rewarding solution (30% sucrose dissolved in water) for 3 consecutive days prior to testing delivered in a plastic weigh boat placed in their homecage. Appetitive conditioning was conducted in the same conditioning chamber and contextual features used for contextual fear conditioning, but with one region of the sidewall replaced with a sucrose reward port (Med Associates; ENV-303LPHD). The receptacle was connected via tubing to a syringe filled with the sucrose reward and loaded in a single speed syringe pump (PHM-200). Each reward was 20 mL in volume. Port entries were detected by breaks of an infrared beam incorporated into the port.

Contextual appetitive conditioning consisted of 30 unsignaled sucrose rewards. Beginning with the start of the trial, rewards were dispensed with an intertrial interval of 45 s + a variable duration defined as follows. Following the intertrial interval, a random number between 1 and 15 was generated after each additional second, and when this number equaled 15 a new trial initiated. Rewards were omitted after 6 (Figures 7F–7J) or 8 (Figures 7A–7E) days of conditioning for extinguished mice and were omitted entirely for unconditioned mice. Unconditioned mice received sucrose solution in their homecage following context exposure. The final test session prior to perfusion for c-Fos analysis was 5 min of context exposure with rewards omitted in all groups. For optogenetic manipulation of SST-INs following appetitive extinction, photoinhibition was delivered for the first 5 min of the 10 min test.

Intersectional activity-dependent neural tagging—Activity-dependent tagging was induced with an intraperitoneal injection of 4-OHT (Sigma) at 10 mg kg^{-1} body weight administered immediately following the behavioral experience of interest (e.g., fear conditioning or extinction retrieval). In Figures 5A–5E, mice were injected with vehicle if not administered 4-OHT. Following 4-OHT injections, mice remained in their homecage in a quiet room for multiple hours in order to minimize non-specific labeling. 4-OHT was first dissolved in dimethyl sulfoxide (DMSO) to a concentration of 40 mg mL^{-1}, then diluted in a 1% Tween-80 solution in sterile saline (0.9%) to a final concentration of 1 mg mL^{-1}.

Tissue preparations and immunohistochemistry—For c-Fos analysis, perfusion began 90 min following context exposure. Mice were deeply anesthetized with isofluorane and transcardially perfused with chilled 1x phosphate buffered saline (PBS) followed by 4% paraformaldehyde (PFA) in 1x PBS. Brains were extracted and post-fixed overnight in 4% PFA at 4°C and then transferred to 30% sucrose in 1x PBS for 2 days at 4°C until saturated. 35 μm coronal sections were collected on a cryostat (Leica Microsystems) and stored in cryoprotectant at −20°C.

For immunohistochemistry, floating sections were washed six times for 5 min in 1x PBS and blocked at room temperature for 1 h in 10% normal goat serum (NGS; Jackson ImmunoResearch; 005-000-121) in 1x PBS with 0.3% Tween 20 (PBST). Sections were incubated with primary antibodies - 1:2000 rabbit anti-cFos (Synaptic Systems; 226 003), 1:500 chicken anti-GFP (Invitrogen; A11122), or 1:1000 rabbit anti-SST (Thermo Fischer Scientific; PA5–82678) - diluted in 5% NGS in 1x PBST overnight at 4°C. Sections were rinsed three times in 1x PBS and incubated in secondary antibodies of 1:500 goat anti-rabbit Alexa Fluor 647 (Jackson ImmunoResearch; 111-605-144) or 1:500 donkey anti-chicken Alexa Fluor 488 (Jackson ImmunoResearch; 703-545-155) in 1x PBST for 2 h at room temperature. Sections were rinsed three times in 1x PBS, mounted onto slides, and coverslipped with ProLong Gold antifade medium containing 4,6-diamidino-2-phenylindole (DAPI; Invitrogen; P36931). All incubations and washes were done with slight agitation on an orbital shaker.

Imaging and cell counting—Fluorescent confocal images of immunolabeled tissue were acquired on a Zeiss LSM 780 with a 20x objective and suitable filter sets in tiled z stack images (4 μm steps) that were stitched using the Zen Black software v. 8.1 (Carl Zeiss). For each experiment, images were acquired with identical laser intensity, gain, and pinhole settings. Immunopositive cell bodies were counted manually in Fiji/ImageJ v.1.53 (NIH)[54] from contours of regions of interest by an experimenter blind to the experimental conditions. Area measurements derived from ImageJ contours was used to calculate estimate of cell count density. To obtain $DAPI^+$ density estimates used in Figure S2, $DAPI^+$ cells were quantified from a selection of 8 sample regions from vCA1 s.p. and s.o. Finally, the mean $DAPI^+$ density estimate from these regions was divided by the total contour area to determine total estimated $DAPI^+$ density for each animal. Mice were excluded from experiments if imaging confirmed off-target optic fiber placement or viral expression.

Electrophysiology—Mice were anesthetized with isoflurane before decapitation. Brains were extracted and submerged in ice-cold, carbogen-bubbled (95% oxygen, 5%CO_2) sucrose cutting solution containing (in mM): 210.3 sucrose, 26.2 $NaHCO_3$, 11 glucose, 2.5 KCl, 1 NaH_2PO_4, 0.5 sodium ascorbate, 4 $MgCl_2$, and 0.5 $CaCl_2$. Horizontal slices containing vCA1 were prepared on a VT1200S Vibratome (Leica Microsystems). Slices were recovered for 40 min at 35°C in carbogen-bubbled artificial cerebrospinal fluid (ACSF) containing (in mM): 119 NaCl, 26.2 $NaHCO_3$, 11 glucose, 2.5 KCl, 1 NaH_2PO_4, 2 $MgCl_2$, and 2 $CaCl_2$. Slices were subsequently maintained and recordings were performed at 24° C. For voltage-clamp recordings, whole-cell electrodes (4–6 MΩ) were pulled from borosilicate glass and filled with a low-chloride internal solution containing (in mM): 120 cesium methanesulfonate, 10 HEPES, 10 sodium phosphocreatine, 8 NaCl, 1 QX-314, 0.5 EGTA, 4 Mg-ATP and 0.4 Na-GTP. The internal solution was adjusted to pH 7.22 and 290–300 mOsm. Slices were visualized on an upright differential interference contrast microscope, and LED-coupled (Prizmatix) 40x objectives were used to identify SST-INs in stratum oriens based on tdTomato fluorescence. Although stratum oriens is devoid of principal excitatory neurons, we relied on the fact that principal excitatory neurons (but not SST-INs) have a prominent apical dendrite extending toward the stratum lacunosum to ensure that they were not accidentally included in our recordings.

Spontaneous and miniature EPSCs and IPSCs were isolated by clamping the neurons at −60 or 0 mV, respectively. A total trace duration of at least 5 min was sampled at each potential for spontaneous currents in normal ACSF, or in 1 μM TTX for miniature currents. Data was low-pass filtered at 3–10 kHz and acquired at 10–20 kHz using Multiclamp 700B Microelectrode Amplifier (Molecular Devices) and pClamp 10 software (Molecular Devices, version 10.3.1). Cells exhibiting low health (<−100 pA holding current), access resistance changes of >20%, or unstable synaptic responses were excluded from the analysis. Event detection and analysis were performed using Easy Electrophysiology v. 2.6.3. Excitatory and inhibitory charge were calculated from an averaged event trace from each cell, which was then multiplied by the event rate to obtain total charge transferred per unit time.

QUANTIFICATION AND STATISTICAL ANALYSIS

Details of statistical tests, including tests performed, F values and any associated p values can be found in the corresponding figure legends. Data that did not meet the assumption of normality as determined by Shapiro-Wilk test were submitted instead to non-parametric analysis (e.g., Kruskal-Wallis ANOVA). All other comparisons were made using parametric analyses (t test, 1-way and 2-way ANOVA, or mixed-effects ANOVA). Following a significant omnibus test, pairwise comparisons among all the groups and/or treatments were used to test for significant differences. No outliers were excluded from any dataset. When data had a normal distribution, they were depicted by mean ± SE. In the case of non-normal distributions, data were described by boxplot depicting minimum and maximum values, 25^{th} and 75^{th} percentiles, and median. Results of all statistical analyses are reported within the corresponding figure legends. Significance (α) was defined as $p < 0.05$. Statistical analyses and figure generation was performed in Prism v.10.2.3 (GraphPad Software), OriginPRO 2019 (OriginLab) and SPSS v. 29.0.2.0 (IBM).

Supplementary Material

Refer to Web version on PubMed Central for supplementary material.

ACKNOWLEDGMENTS

These experiments were supported by the following grants from the National Institute of Mental Health to R.L.C. (R01 MH116445, R01 MH124880, and R01 MH132224) and a graduate research fellowship from the National Science Foundation to T.N.D. The icons used in Figures 1A, 1G, 2A, 4C, and 6A were made with BioRender. We thank members of the Clem lab for feedback on the manuscript.

REFERENCES

1. Milton AL, and Everitt BJ (2012). The persistence of maladaptive memory: addiction, drug memories and anti-relapse treatments. Neurosci. Biobehav. Rev. 36, 1119–1139. 10.1016/j.neubiorev.2012.01.002. [PubMed: 22285426]
2. Orsini CA, and Maren S (2012). Neural and cellular mechanisms of fear and extinction memory formation. Neurosci. Biobehav. Rev. 36, 1773–1802. 10.1016/j.neubiorev.2011.12.014. [PubMed: 22230704]
3. Goode TD, and Maren S (2019). Common neurocircuitry mediating drug and fear relapse in preclinical models. Psychopharmacology (Berl) 236, 415–437. 10.1007/s00213-018-5024-3. [PubMed: 30255379]

4. Sevenster D, Visser RM, and D'Hooge R (2018). A translation alperspective on neural circuits of fear extinction: Current promises and challenges. Neurobiol. Learn. Mem. 155, 113–126. 10.1016/j.nlm.2018.07.002. [PubMed: 29981423]
5. Singewald N, and Holmes A (2019). Rodent models of impaired fear extinction. Psychopharmacology (Berl) 236, 21–32. 10.1007/s00213-018-5054-x. [PubMed: 30377749]
6. Venniro M, Caprioli D, and Shaham Y (2016). Animal models of drug relapse and craving: From drug priming-induced reinstatement to incubation of craving after voluntary abstinence. Prog. Brain Res. 224, 25–52. 10.1016/bs.pbr.2015.08.004. [PubMed: 26822352]
7. Chaaya N, Battle AR, and Johnson LR (2018). An update on contextual fear memory mechanisms: Transition between Amygdala and Hippocampus. Neurosci. Biobehav. Rev. 92, 43–54. 10.1016/j.neubiorev.2018.05.013. [PubMed: 29752958]
8. Smith DM, Yang YY, Subramanian DL, Miller AMP, Bulkin DA, and Law LM (2022). The limbic memory circuit and the neural basis of contextual memory. Neurobiol. Learn. Mem. 187, 107557. 10.1016/j.nlm.2021.107557. [PubMed: 34808337]
9. Goode TD, and Maren S (2014). Animal models of fear relapse. ILAR J. 55, 246–258. 10.1093/ilar/ilu008. [PubMed: 25225304]
10. Clem RL, and Schiller D (2016). New Learning and Unlearning: Strangers or Accomplices in Threat Memory Attenuation? Trends Neurosci. 39, 340–351. 10.1016/j.tins.2016.03.003. [PubMed: 27079843]
11. Grewe BF, Grundemann J, Kitch LJ, Lecoq JA, Parker JG, Marshall JD, Larkin MC, Jercog PE, Grenier F, Li JZ, et al. (2017). Neural ensemble dynamics underlying a long-term associative memory. Nature 543, 670–675. 10.1038/nature21682. [PubMed: 28329757]
12. Herry C, Ciocchi S, Senn V, Demmou L, Müller C, and Lüthi A (2008). Switching on and off fear by distinct neuronal circuits. Nature 454, 600–606. 10.1038/nature07166. [PubMed: 18615015]
13. Lacagnina AF, Brockway ET, Crovetti CR, Shue F, McCarty MJ, Sattler KP, Lim SC, Santos SL, Denny CA, and Drew MR (2019). Distinct hippocampal engrams control extinction and relapse of fear memory. Nat. Neurosci. 22, 753–761. 10.1038/s41593-019-0361-z. [PubMed: 30936555]
14. Wang G, Xie H, Wang L, Luo W, Wang Y, Jiang J, Xiao C, Xing F, and Guan JS (2019). Switching From Fear to No Fear by Different Neural Ensembles in Mouse Retrosplenial Cortex. Cereb. Cortex 29, 5085–5097. 10.1093/cercor/bhz050. [PubMed: 30888026]
15. Zaki Y, Mau W, Cincotta C, Monasterio A, Odom E, Doucette E, Grella SL, Merfeld E, Shpokayte M, and Ramirez S (2022). Hippocampus and amygdala fear memory engrams re-emerge after contextual fear relapse. Neuropsychopharmacology 47, 1992–2001. 10.1038/s41386-022-01407-0. [PubMed: 35941286]
16. Zhang X, Kim J, and Tonegawa S (2020). Amygdala Reward Neurons Form and Store Fear Extinction Memory. Neuron 105, 1077–1093.e7. 10.1016/j.neuron.2019.12.025. [PubMed: 31952856]
17. Schuette PJ, Reis FMCV, Maesta-Pereira S, Chakerian M, Torossian A, Blair GJ, Wang W, Blair HT, Fanselow MS, Kao JC, and Adhikari A (2020). Long-Term Characterization of Hippocampal Remapping during Contextual Fear Acquisition and Extinction. J. Neurosci. 40, 8329–8342. 10.1523/JNEUROSCI.1022-20.2020. [PubMed: 32958567]
18. Tanaka KZ, He H, Tomar A, Niisato K, Huang AJY, and McHugh TJ (2018). The hippocampal engram maps experience but not place. Science 361, 392–397. 10.1126/science.aat5397. [PubMed: 30049878]
19. Tronson NC, Schrick C, Guzman YF, Huh KH, Srivastava DP, Penzes P, Guedea AL, Gao C, and Radulovic J (2009). Segregated populations of hippocampal principal CA1 neurons mediating conditioning and extinction of contextual fear. J. Neurosci. 29, 3387–3394. 10.1523/JNEUROSCI.5619-08.2009. [PubMed: 19295145]
20. Wang ME, Yuan RK, Keinath AT, Ramos Álvarez MM, and Muzzio IA (2015). Extinction of Learned Fear Induces Hippocampal Place Cell Remapping. J. Neurosci. 35, 9122–9136. 10.1523/JNEUROSCI.4477-14.2015. [PubMed: 26085635]
21. Artinian J, Jordan A, Khlaifia A, Honoré E, La Fontaine A, Racine AS, Laplante I, and Lacaille JC (2019). Regulation of Hippocampal Memory by mTORC1 in Somatostatin Interneurons. J. Neurosci. 39, 8439–8456. 10.1523/JNEUROSCI.0728-19.2019. [PubMed: 31519824]

22. Cummings KA, Bayshtok S, Dong TN, Kenny PJ, and Clem RL(2022). Control of fear by discrete prefrontal GABAergic populations encoding valence-specific information. Neuron 110, 3036–3052.e5. 10.1016/j.neuron.2022.07.004. [PubMed: 35944526]
23. Cummings KA, and Clem RL (2020). Prefrontal somatostatin interneurons encode fear memory. Nat. Neurosci. 23, 61–74. 10.1038/s41593-019-0552-7 . [PubMed: 31844314]
24. Schmid LC, Mittag M, Poll S, Steffen J, Wagner J, Geis HR, Schwarz I, Schmidt B, Schwarz MK, Remy S, and Fuhrmann M (2016). Dysfunction of Somatostatin-Positive Interneurons Associated with Memory Deficits in an Alzheimer's Disease Model. Neuron 92, 114–125. 10.1016/j.neuron.2016.08.034. [PubMed: 27641495]
25. Sharma V, Sood R, Khlaifia A, Eslamizade MJ, Hung TY, Lou D, Asgarihafshejani A, Lalzar M, Kiniry SJ, Stokes MP, et al. (2020). eIF2alpha controls memory consolidation via excitatory and somatostatin neurons. Nature 586, 412–416. 10.1038/s41586-020-2805-8. [PubMed: 33029011]
26. Stefanelli T, Bertollini C, Lüscher C, Muller D, and Mendez P (2016). Hippocampal Somatostatin Interneurons Control the Size of Neuronal Memory Ensembles. Neuron 89, 1074–1085. 10.1016/j.neuron.2016.01.024. [PubMed: 26875623]
27. Stujenske JM, O'Neill PK, Fernandes-Henriques C, Nahmoud I, Goldburg SR, Singh A, Diaz L, Labkovich M, Hardin W, Bolkan SS, et al. (2022). Prelimbic cortex drives discrimination of non-aversion via amygdala somatostatin interneurons. Neuron 110, 2258–2267.e2211. 10.1016/j.neuron.2022.03.020. [PubMed: 35397211]
28. Xu H, Liu L, Tian Y, Wang J, Li J, Zheng J, Zhao H, He M, Xu TL, Duan S, and Xu H (2019). A Disinhibitory Microcircuit Mediates Conditioned Social Fear in the Prefrontal Cortex. Neuron 102, 668–682.e5. 10.1016/j.neuron.2019.02.026. [PubMed: 30898376]
29. Funk CM, Peelman K, Bellesi M, Marshall W, Cirelli C, and Tononi G (2017). Role of Somatostatin-Positive Cortical Interneurons in the Generation of Sleep Slow Waves. J. Neurosci. 37, 9132–9148. 10.1523/JNEUROSCI.1303-17.2017. [PubMed: 28821651]
30. Kim T, Choi DI, Choi JE, Lee H, Jung H, Kim J, Sung Y, Park H, Kim MJ, Han DH, et al. (2024). Activated somatostatin interneurons orchestrate memory microcircuits. Neuron 112, 201–208.e4. 10.1016/j.neuron.2023.10.013. [PubMed: 37944516]
31. Tossell K, Yu X, Giannos P, Anuncibay Soto B, Nollet M, Yustos R, Miracca G, Vicente M, Miao A, Hsieh B, et al. (2023). Somatostatin neurons in prefrontal cortex initiate sleep-preparatory behavior and sleep via the preoptic and lateral hypothalamus. Nat. Neurosci. 26, 1805–1819. 10.1038/s41593-023-01430-4. [PubMed: 37735497]
32. Tovote P, Fadok JP, and Luthi A (2015). Neuronal circuits for fear and€ anxiety. Nat. Rev. Neurosci. 16, 317–331. 10.1038/nrn3945. [PubMed: 25991441]
33. Honore E, Khlaifia A, Bosson A, and Lacaille JC (2021). Hippocampal Somatostatin Interneurons, Long-Term Synaptic Plasticity and Memory. Front Neural Circuits 15, 687558. 10.3389/fncir.2021.687558. [PubMed: 34149368]
34. Drexel M, Rahimi S, and Sperk G (2022). Silencing of Hippocampal Somatostatin Interneurons Induces Recurrent Spontaneous Limbic Seizures in Mice. Neuroscience 487, 155–165. 10.1016/j.neuroscience.2022.02.007. [PubMed: 35167940]
35. Muller-Komorowska D, Opitz T, Elzoheiry S, Schweizer M, Ambrad Giovannetti E, and Beck H (2020). Nonspecific Expression in Limited Excitatory Cell Populations in Interneuron-Targeting Cre-driver Lines Can Have Large Functional Effects. Front Neural Circuits 14, 16. 10.3389/fncir.2020.00016. [PubMed: 32395103]
36. Asgarihafshejani A, Honoré É, Michon FX, Laplante I, and Lacaille JC (2022). Long-term potentiation at pyramidal cell to somatostatin interneuron synapses controls hippocampal network plasticity and memory. iScience 25, 104259. 10.1016/j.isci.2022.104259. [PubMed: 35521524]
37. Kawashima T, Kitamura K, Suzuki K, Nonaka M, Kamijo S, Takemoto-Kimura S, Kano M, Okuno H, Ohki K, and Bito H (2013). Functional labeling of neurons and their projections using the synthetic activity-dependent promoter E-SARE. Nat. Methods 10, 889–895. 10.1038/nmeth.2559. [PubMed: 23852453]
38. Tzilivaki A, Tukker JJ, Maier N, Poirazi P, Sammons RP, and Schmitz D (2023). Hippocampal GABAergic interneurons and memory. Neuron 111, 3154–3175. 10.1016/j.neuron.2023.06.016. [PubMed: 37467748]

39. Suthard RL, Senne RA, Buzharsky MD, Diep AH, Pyo AY, and Ramirez S (2024). Engram reactivation mimics cellular signatures of fear. Cell Rep. 43, 113850. 10.1016/j.celrep.2024.113850. [PubMed: 38401120]
40. Leao RN, Mikulovic S, Leao KE, Munguba H, Gezelius H, Enjin A, Patra K, Eriksson A, Loew LM, Tort AB, and Kullander K (2012). OLM interneurons differentially modulate CA3 and entorhinal inputs to hippocampal CA1 neurons. Nat. Neurosci. 15, 1524–1530. 10.1038/nn.3235. [PubMed: 23042082]
41. Nichol H, Amilhon B, Manseau F, Badrinarayanan S, and Williams S (2018). Electrophysiological and Morphological Characterization of Chrna2 Cells in the Subiculum and CA1 of the Hippocampus: An Optogenetic Investigation. Front. Cell. Neurosci. 12, 32. 10.3389/fncel.2018.00032. [PubMed: 29487503]
42. Grienberger C, and Magee JC (2022). Entorhinal cortex directs learning-related changes in CA1 representations. Nature 611, 554–562. 10.1038/s41586-022-05378-6. [PubMed: 36323779]
43. Chamberland S, Grant G, Machold R, Nebet ER, Tian G, Hanani M, Kullander K, and Tsien RW (2023). Functional specialization of hippocampal somatostatin-expressing interneurons. Preprint at: bioRxiv, 2023.04.27.538511. 10.1101/2023.04.27.538511
44. Cope DW, Maccaferri G, Márton LF, Roberts JDB, Cobden PM, and Somogyi P (2002). Cholecystokinin-immunopositive basket and Schaffer collateral-associated interneurones target different domains of pyramidal cells in the CA1 area of the rat hippocampus. Neuroscience 109, 63–80. 10.1016/s0306-4522(01)00440-7. [PubMed: 11784700]
45. Vida I, Halasy K, Szinyei C, Somogyi P, and Buhl EH (1998). Unitary IPSPs evoked by interneurons at the stratum radiatum-stratum lacunosum-moleculare border in the CA1 area of the rat hippocampus in vitro. J. Physiol. 506 (Pt 3), 755–773. 10.1111/j.1469-7793.1998.755bv.x. [PubMed: 9503336]
46. Yassa MA, and Stark CEL (2011). Pattern separation in the hippocampus. Trends Neurosci. 34, 515–525. 10.1016/j.tins.2011.06.006. [PubMed: 21788086]
47. Mikulovic S, Restrepo CE, Siwani S, Bauer P, Pupe S, Tort ABL, Kullander K, and Leão RN (2018). Ventral hippocampal OLM cells control type 2 theta oscillations and response to predator odor. Nat. Commun. 9, 3638. 10.1038/s41467-018-05907-w. [PubMed: 30194386]
48. Totty MS, Tuna T, Ramanathan KR, Jin J, Peters SE, and Maren S (2023). Thalamic nucleus reuniens coordinates prefrontal-hippocampal synchrony to suppress extinguished fear. Nat. Commun. 14, 6565. 10.1038/s41467-023-42315-1. [PubMed: 37848425]
49. Lovett-Barron M, Kaifosh P, Kheirbek MA, Danielson N, Zaremba JD, Reardon TR, Turi GF, Hen R, Zemelman BV, and Losonczy A (2014). Dendritic inhibition in the hippocampus supports fear learning. Science 343, 857–863. 10.1126/science.1247485. [PubMed: 24558155]
50. Ogando MB, Pedroncini O, Federman N, Romano SA, Brum LA, Lanuza GM, Refojo D, and Marin-Burgin A (2021). Cholinergic modulation of dentate gyrus processing through dynamic reconfiguration of inhibitory circuits. Cell Rep. 36, 109572. 10.1016/j.celrep.2021.109572. [PubMed: 34433032]
51. Biane JS, Ladow MA, Stefanini F, Boddu SP, Fan A, Hassan S, Dundar N, Apodaca-Montano DL, Zhou LZ, Fayner V, et al. (2023). Neural dynamics underlying associative learning in the dorsal and ventral hippocampus. Nat. Neurosci. 26, 798–809. 10.1038/s41593-023-01296-6. [PubMed: 37012382]
52. Bernier BE, Lacagnina AF, and Drew MR (2014). Potent attenuation of context fear by extinction training contiguous with acquisition. Learn. Mem. 22, 31–38. 10.1101/lm.036673.114. [PubMed: 25512575]
53. Bruno CA, O'Brien C, Bryant S, Mejaes JI, Estrin DJ, Pizzano C, and Barker DJ (2021). pMAT: An open-source software suite for the analysis of fiber photometry data. Pharmacol. Biochem. Behav. 201, 173093. 10.1016/j.pbb.2020.173093. [PubMed: 33385438]
54. Schindelin J, Arganda-Carreras I, Frise E, Kaynig V, Longair M, Pietzsch T, Preibisch S, Rueden C, Saalfeld S, Schmid B, et al. (2012). Fiji: an open-source platform for biological-image analysis. Nat. Methods 9, 676–682. 10.1038/nmeth.2019. [PubMed: 22743772]

Highlights

- Contextual fear extinction activates ventral CA1 (vCA1) somatostatin interneurons (SST-INs)
- vCA1 SST-IN activity is organized around defensive freezing bouts
- SST-IN but not PV-IN activity controls contextual fear extinction and relapse
- Extinction of appetitive contextual associations exhibits similar requirement for SST-Ins

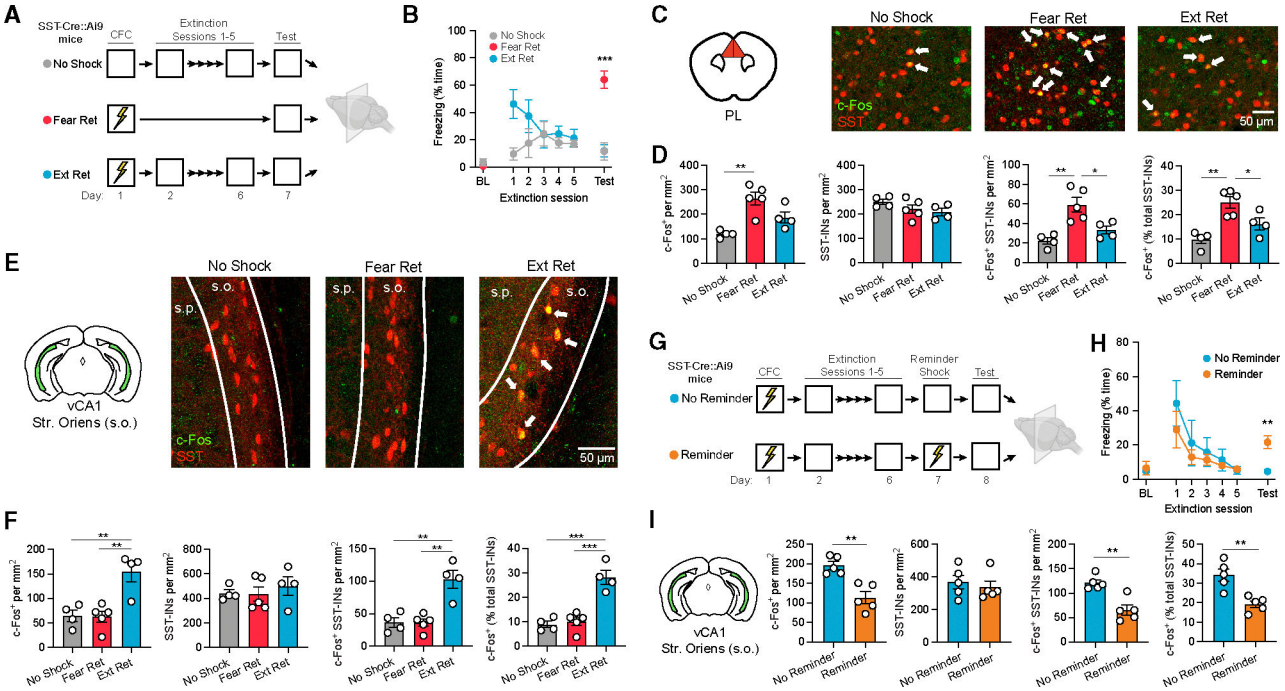

Figure 1. Extinction modulates context-evoked activity of prelimbic and vCA1 SST-Ins

(A) Design for analysis of c-Fos expression following retrieval of contextual fear extinction (Ext Ret) as compared to control subjects for which either foot shocks (No Shock) or extinction (Fear Ret) were omitted. Contextual fear conditioning (CFC) consisted of three 2 s, 0.75 mA shocks, and extinction consisted of 10 min of context exposure daily for 5 days. Brains were collected for immunohistochemical analysis 90 min following a final context test (5 min). All mice were SST-Cre::Ai9.

(B) Freezing across extinction and test sessions. BL, preconditioning baseline. Freezing during test: $F_{(2, 10)} = 26.8$, $p < 0.0001$, one-way ANOVA.

(C) c-Fos (red) and SST-IN (green) labeling for the PL. Arrows denote co-labeled cells.

(D) Group comparisons of prelimbic cell counts by one-way ANOVA. c-Fos$^+$ cell density: $F_{(2, 10)} = 11.8$, $p < 0.01$. c-Fos$^+$ SST-IN density: $F_{(2, 10)} = 11.4$, $p < 0.01$. c-Fos$^+$ SST-INs (% total SST-INs): $F_{(2, 10)} = 12.3$, $p < 0.01$.

(E) c-Fos and SST labeling for the vCA1 stratum oriens (s.o.). Arrows denote co-labeled cells.

(F) Group comparisons of vCA1 s.o. cell counts by one-way ANOVA. c-Fos$^+$ cell density: $F_{(2, 10)} = 11.11$, $p < 0.01$. c-Fos$^+$ SST-IN density: $F_{(2, 10)} = 14.17$, $p < 0.01$. c-Fos$^+$ SST-INs (% total SST-INs): $F_{(2, 10)} = 27.10$, $p < 0.0001$.

(G) Design for analysis of c-Fos expression following reminder shock-induced relapse. Subjects were treated identically throughout CFC and extinction, except one group was exposed to a single reminder shock prior to the test (Reminder).

(H) Freezing across extinction and test sessions. Freezing during test: $t_{(8)} = 4.27$, $p < 0.01$.

(I) Group comparisons of vCA1 s.o. immunohistochemical cell counts by unpaired t test. c-Fos$^+$ cell density: $t_{(8)} = 4.50$, $p < 0.01$. c-Fos$^+$ SST-IN density: $t_{(8)} = 4.58$, $p < 0.01$. c-Fos$^+$ SST-INs (% total SST-INs): $t(8) = 4.17$, $p < 0.01$.

(A–F) No Shock: $n = 4$; Fear Ret: $n = 5$; Ext Ret: n = 4.

(G–I) Ext Ret: $n = 5$; Reminder: $n = 5$.

$^{*}p < 0.05$, $^{**}p < 0.01$, $^{***}p < 0.001$ by Tukey's post hoc test (B, D, and F) or unpaired t test (H and I). Error bars indicate standard error of mean.

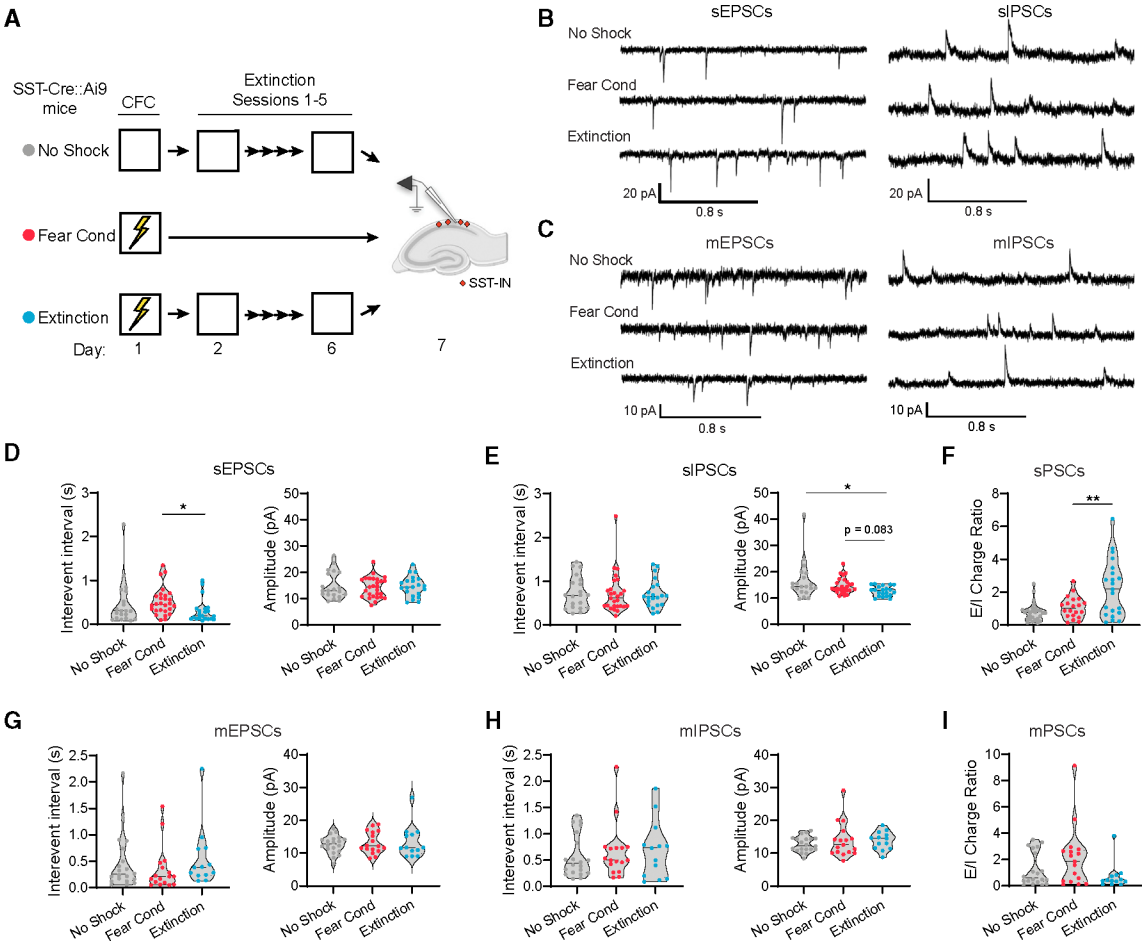

Figure 2. Extinction increases the excitatory:inhibitory balance of spontaneous but not miniature postsynaptic currents in vCA1 SST-Ins

(A) Design for analysis of synaptic transmission using whole-cell electrophysiology following extinction (Extinction) as compared to control subjects for which foot shocks (No Shock) or extinction (Fear Cond) were omitted. All mice were SST-Cre::Ai9.

(B) Representative current traces containing spontaneous EPSCs (sEPSCs) and sIPSCs, which were sampled from the same population of SST-INs.

(C) Representative current traces containing miniature EPSCs (mEPSCs) and miniature IPSCs (mIPSCs), which were sampled from the same population of SST-INs in the presence of 1 μm TTX.

(D) Group comparison of sEPSC properties by Kruskal-Wallis ANOVA. Interevent interval: $\chi^2 = 8.14$, $p < 0.05$.

(E) Group comparison of sIPSC properties by Kruskal-Wallis ANOVA. Amplitude: $\chi^2 = 7.91$, $p < 0.05$.

(F) Group comparison of sEPSC charge normalized to sIPSC charge for individual SST-INs (E/I ratio) by Kruskal-Wallis ANOVA. Charge (Q) is calculated as the total area of spontaneous currents per second of recording. E/I ratio: $\chi^2 = 10.4$, $p < 0.01$.

(G) Group comparison of mEPSC properties.

(H) Group comparison of mIPSC properties.

(I) Group comparison of mEPSC charge normalized to mIPSC charge for individual SST-INs (E/I ratio). (D–F) No Shock: $n = 20$ cells (6 mice); Fear Cond: $n = 27$ (4 mice); Extinction: $n = 21$ cells (5 mice).
(G–I) No Shock: $n = 20$ cells (5 mice); Fear Cond: $n = 17$ cells (5 mice); Extinction: $n = 13$ cells (3 mice).
*$p < 0.05$, **$p < 0.01$ by Dunn's post hoc test.

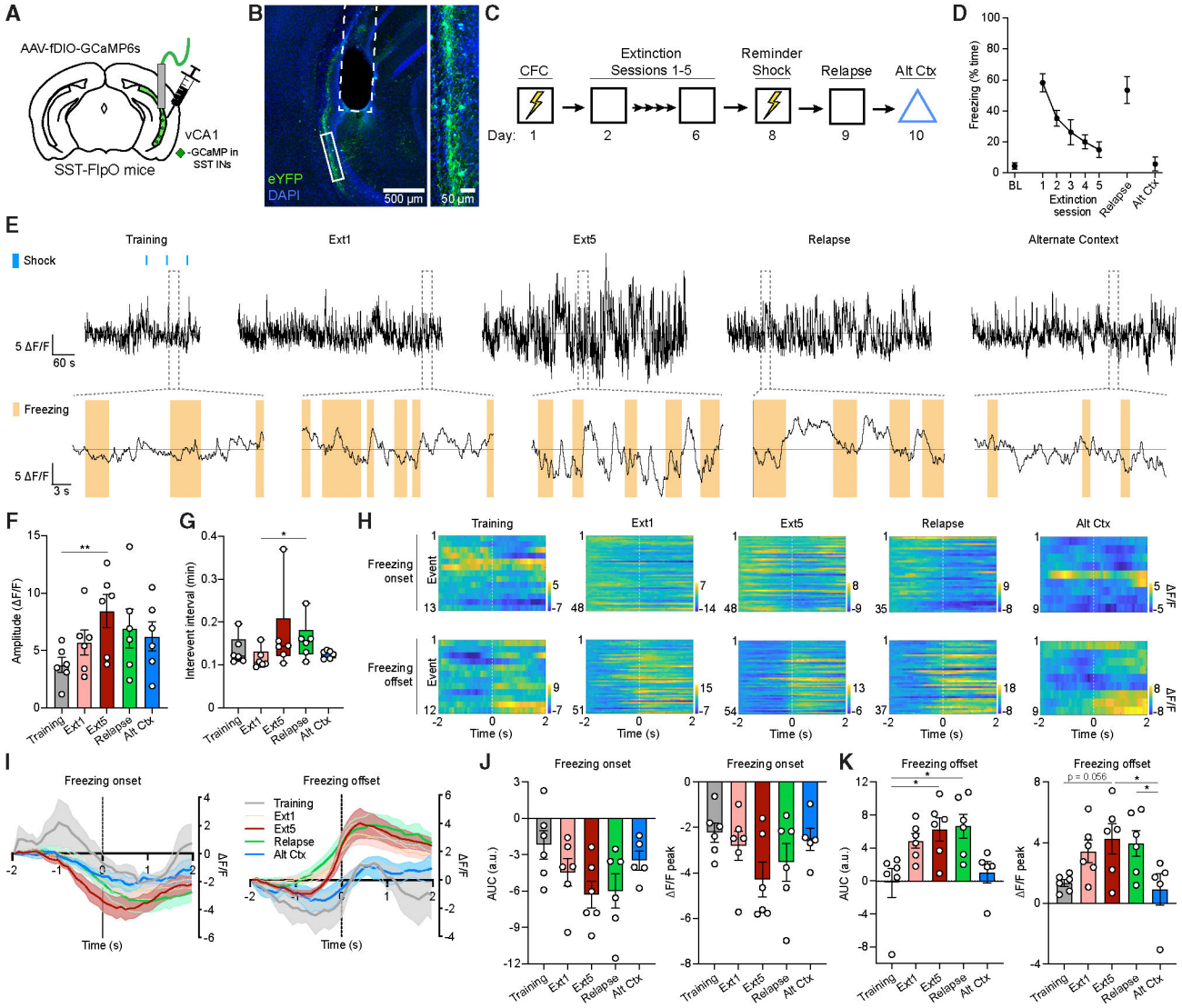

Figure 3. *In vivo* vCA1 SST-IN activity is organized around freezing bouts and amplified by extinction

(A) Strategy for fiber photometry recordings in vCA1 SST-INs in SST-FlpO mice.

(B) Representative image of GCaMP6s viral expression and optic fiber placement (dashed white line). A solid white box indicates the area of magnification (right).

(C) Design for fiber photometry recording across CFC, extinction, reminder shock-induced relapse, and alternate context exposure.

(D) Freezing during preconditioning BL, extinction sessions, relapse, and alternate context tests.

(E) Top row: representative whole session normalized Ca^{2+} activity (reported as ΔF/F) from vCA1 SST-INs. Blue boxes indicate foot shocks during training. Bottom row: expanded calcium traces from areas highlighted by dashed gray boxes, with freezing bouts ≥1 s indicated by orange boxes.

(F) Whole-session analysis of peak Ca^{2+} event amplitude (ΔF/F) by one-way repeated measures ANOVA. $F_{(4, 20)} = 4.60$, $p < 0.01$.

(G) Whole-session analysis of interevent interval by Friedman test. $\chi^2 = 9.85$, $p < 0.05$.
(H) Representative peri-event time heatmaps (PETH) of Ca^{2+} activity (ΔF/F) across sessions of ±2 s from freezing onset (top row) and freezing offset (bottom row) events.
(I) Mean ΔF/F across sessions of ±2 s from freezing onset (left) and freezing offset (right) events.
(J and K) Quantification of area under the curve (AUC) (left) and peak amplitude (right) of mean ΔF/F across sessions of 0–2 s from freezing onset (J) and freezing offset (K) events, as analyzed by mixed-effects model analysis. Freezing offset AUC: $F_{(4, 19)} = 5.43$, $p < 0.01$. Freezing offset peak: $F_{(4, 19)} = 4.89$, $p < 0.01$. $n = 6$; one mouse did not have any freezing bouts that met inclusion criteria for PETH analysis in the Alt Ctx test, and thus a mixed-effects model was used to handle this omission.
*$p < 0.05$, **$p < 0.01$ by Tukey's post hoc test (F, J, and K) or Dunn's post hoc test (G). Error bars indicate standard error of mean.

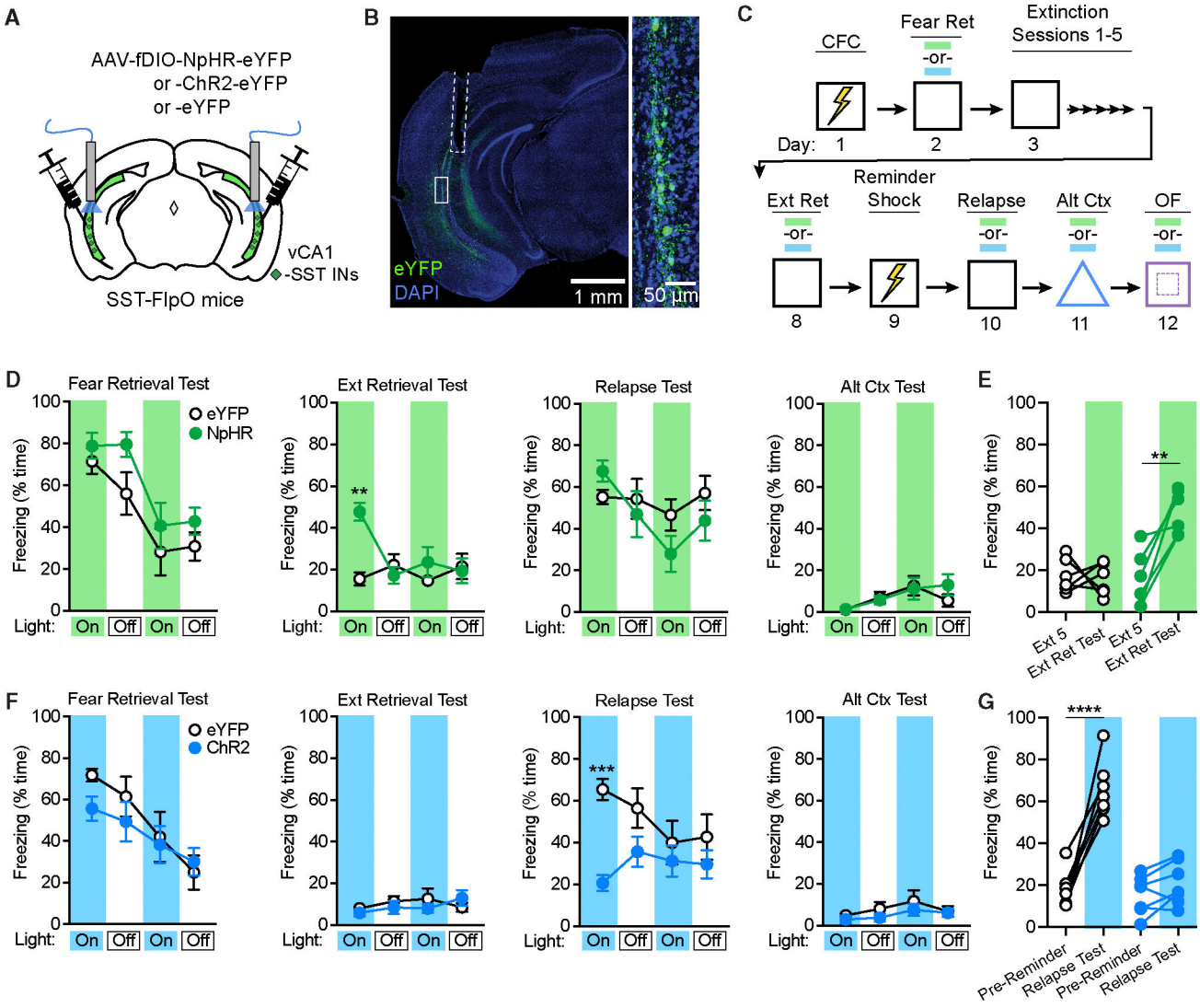

Figure 4. Manipulation of SST-IN activity alters freezing to the conditioned context following extinction

(A) Strategy for targeting of vCA1 SST-INs for optogenetic manipulations with halorhodopsin (NpHR), channelrhodopsin-2 (ChR2), or opsin-negative controlvectors (eYFP only) in SST-FlpO mice.

(B) Representative image of resulting viral expression and optic fiber placement (dashed white line). A solid white box indicates the area of magnification (right).

(C) Design for CFC, extinction, reminder shock-induced relapse, and alternate context exposure with photostimulation tests at the indicated time points (blue and green bars). OF, open field test.

(D) Effect of NpHR-mediated photoinhibition during fear retrieval, extinction retrieval, relapse, and alternate context tests, as analyzed by two-way repeated-measures ANOVA across all light-on and light-off epochs (3 min duration), of which there were two light-on and light-off epochs per session. Opsin 3 epoch interaction: $F_{(15, 150)} = 2.40$, $p < 0.01$.

(E) Change in freezing between the first 3 min of the final extinction session (Ext 5) and the first light-on epoch of the extinction retrieval test (Ext Ret Test), as analyzed by two-way repeated measures ANOVA. Opsin × test interaction: $F_{(1, 10)} = 11.1$, $p < 0.01$.
(F) Effect of ChR2-mediated photoexcitation during similar tests as in (D), as analyzed by two-way repeated-measures ANOVA across all light-on and light-offepochs. Opsin × epoch interaction: $F_{(15, 180)} = 3.01$, $p < 0.001$.
(G) Change in freezing between the pre-reminder shock BL period and first light-on epoch of the relapse test. Opsin × test interaction: $F_{(1, 12)} = 35.7$, $p < 0.0001$. eYFP for NpHR experiment: $n = 6$; NpHR: $n = 6$; eYFP for ChR2 experiment: $n = 7$; ChR2: $n = 7$.
$^{**}p < 0.01$, $^{***}p < 0.001$ by Tukey's post hoc test (D and F) or Šídák's post hoc test (E and G). Error bars indicate standard error of mean.

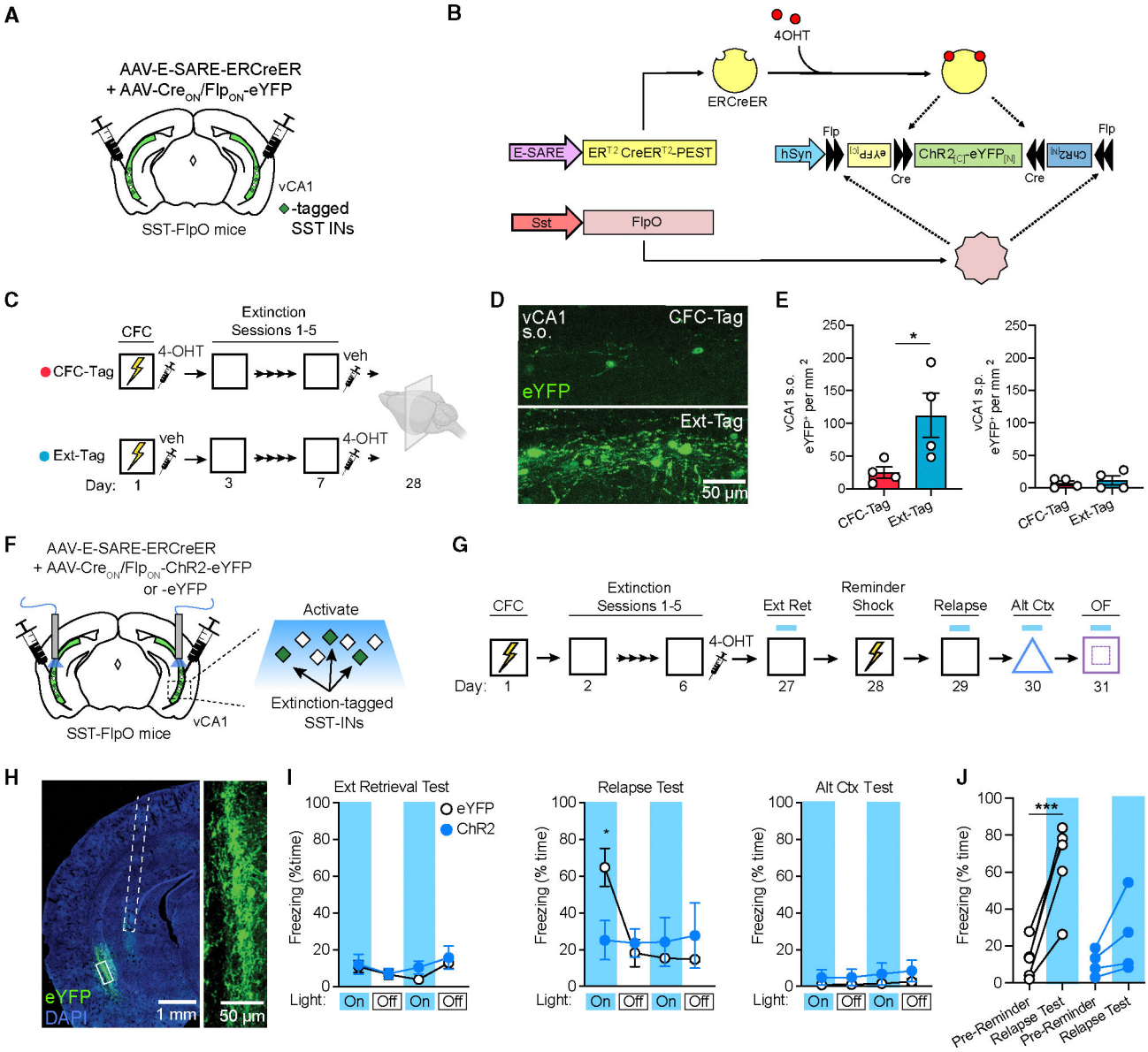

Figure 5. Selective reactivation of extinction-related SST-INs is sufficient to prevent the return of fear

(A) Strategy for selective targeting of vCA1 extinction-related SST-INs for expression of eYFP.

(B) Infusion of a viral cocktail into SST-FlpO mice enables intersectional tagging of recently activated SST-INs, temporally restricted by systemic 4-OHT injection.

(C) Design for SST-IN tagging coinciding with CFC (FC-Tag) or late extinction (Ext-Tag), in which mice were immediately injected with 4-OHT following either session.

(D) Representative images of eYFP tagging in the s.o. of the vCA1.

(E) eYFP$^+$ cell density within the s.o. (left) or stratum pyramidale (s.p.; right). vCA1 s.o. eYFP$^+$ cell density: $t_{(6)} = 2.51$, $p < 0.05$.

(F) Strategy for targeting of extinction-related vCA1 SST-INs for optogenetic manipulations with channelrhodopsin-2 (ChR2) or opsin-negative control vectors (eYFP only) in SST-FlpO mice.
(G) Design for fear conditioning, extinction, reminder shock-induced relapse, and alternate context exposure with photostimulation tests at the indicated time points.
(H) Representative image of resulting viral expression and optic fiber placement (dashed white line). A solid white box indicates the area of magnification (right).
(I) Effect of ChR2-mediated photoexcitation during extinction retrieval, relapse, and alternate context tests, as analyzed by two-way repeated-measures ANOVA across all light-on and light-off epochs (3 min duration). Opsin × epoch interaction: $F_{(11, 77)} = 3.44$, $p < 0.001$.
(J) Change in freezing between the pre-reminder shock BL period and first light-on epoch of the relapse test. Opsin × test interaction: $F_{(1, 7)} = 11.7$, $p < 0.05$.
(A–E) FC-Tag: $n = 5$; Ext-Tag: $n = 4$.
(F–J) eYFP: $n = 5$; ChR2: $n = 4$.
*$p < 0.05$, ***$p < 0.001$ by unpaired t test (E), Tukey's post hoc test (I), or Šídák's post hoc test (J). Error bars indicate standard error of mean.

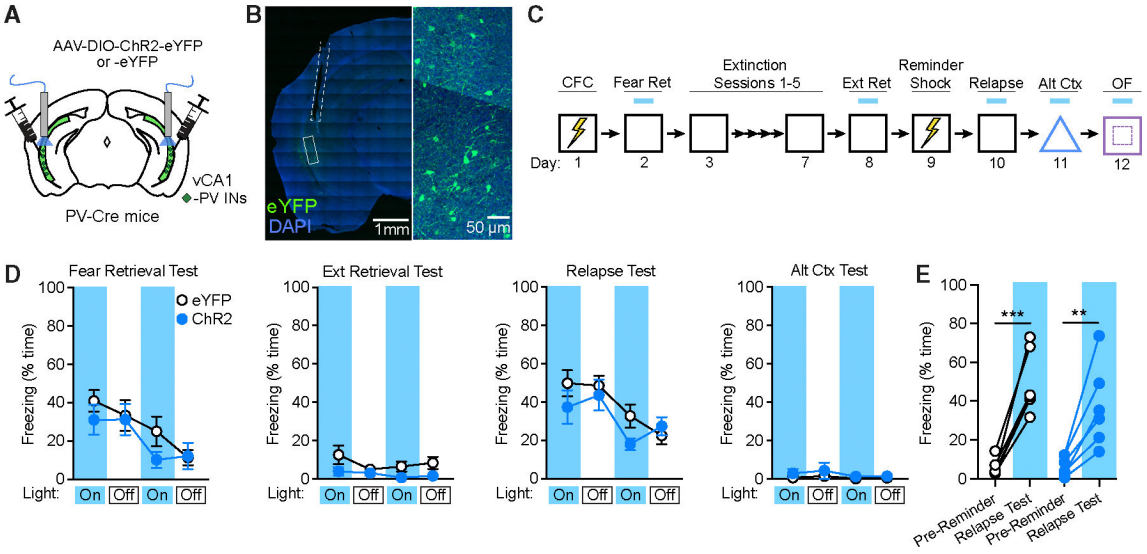

Figure 6. Context fear is unaffected by activation of vCA1 PV-Ins

(A) Strategy for targeting of vCA1 PV-INs for photoexcitation with channelrhodopsin-2 (ChR2) or opsin-negative control vectors (eYFP only) in PV-Cre mice.

(B) Representative image of viral expression and optic fiber placement (dashed white line). A solid white box indicates the area of magnification (right).

(C) Design for CFC, extinction, reminder shock-induced relapse, and alternate context exposure, with photoexcitation tests at the indicated time points.

(D) No effect of ChR2-mediated photoexcitation during fear retrieval, extinction retrieval, relapse, and alternate context tests as analyzed by two-way repeated-measures ANOVA across all light-on and light-off epochs.

(E) Change in freezing between the pre-reminder shock BL period and first light-on epoch of the relapse test was not modulated by opsin expression. eYFP: $n = 6$; ChR2: $n = 6$. $^{**}p < 0.01$, $^{***}p < 0.001$ by Šídák's post hoc test. Error bars indicate standard error of mean.

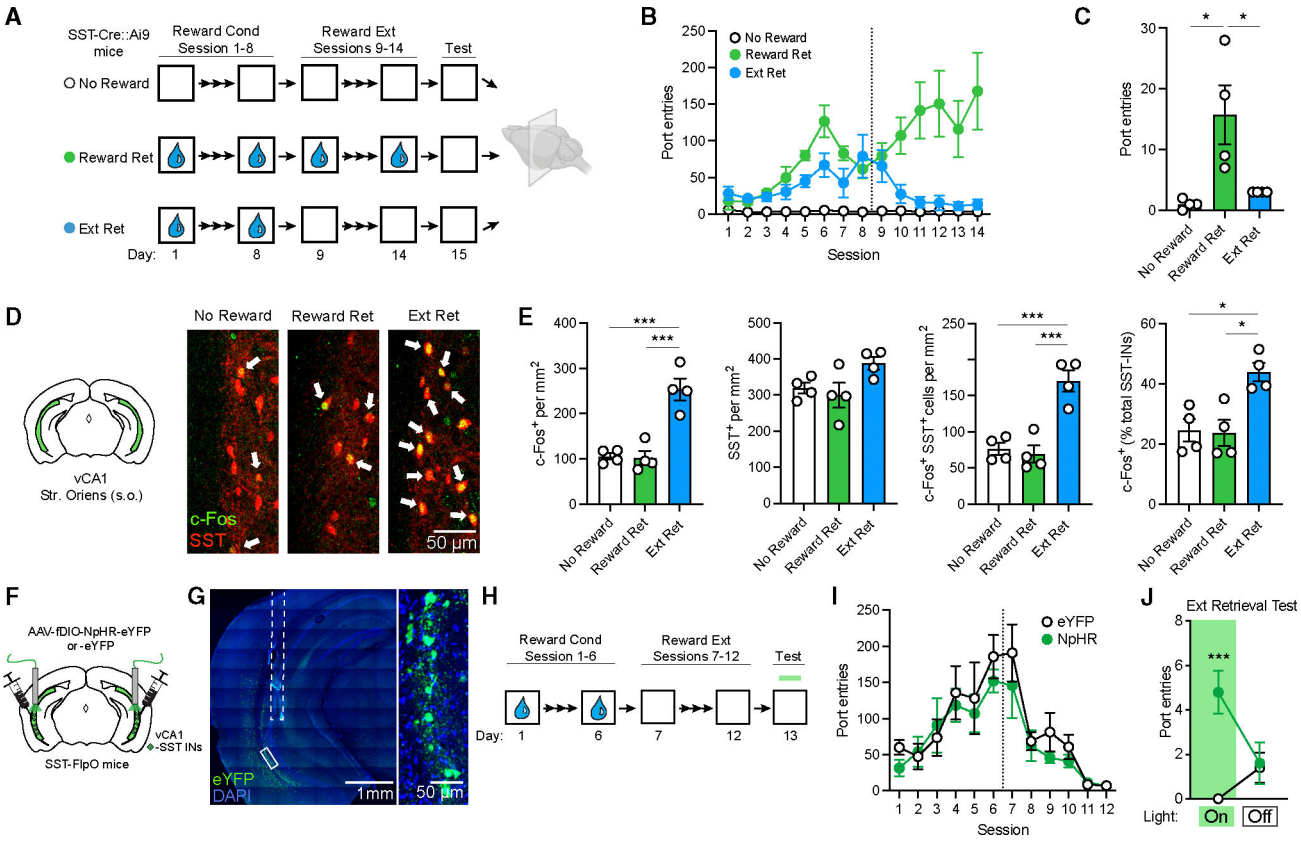

Figure 7. Extinction retrieval after appetitive conditioning depends on vCA1 SST-IN activity

(A) Design for analysis of c-Fos expression following retrieval of contextual reward extinction (Ext Ret) as compared to control subjects for which either sucrose reward (No Reward) or extinction (Reward Ret) were omitted. Appetitive conditioning consisted of unsignaled delivery of 30% sucrose to a reward port 30 times a session at a variable interval (with total session length of ~30 min). Brains were collected for immunohistochemical analysis 90 min following a final context test (5 min) without reward delivery. All mice were SST-Cre::Ai9.

(B) Group comparison of entries into the sucrose delivery port as a function of conditioning and extinction.

(C) Port entries during 5 min context test where sucrose was omitted in all groups. Port entries during test: $\chi^2 = 10.2$, $p < 0.001$, Kruskal-Wallis ANOVA.

(D) c-Fos (red) and SST (green) labeling in the vCA1. Arrows indicate co-labeled cells.

(E) Group comparisons of vCA1 s.o. cell counts by one-way ANOVA. c-Fos$^+$ cell density: $F_{(2, 9)} = 25.8$, $p < 0.001$. c-Fos$^+$/SST-IN density: $F_{(2, 9)} = 22.4$, $p < 0.001$. c-Fos$^+$ SST-INs (% total SST-INs): $F_{(2, 9)} = 9.40$, $p < 0.01$.

(F) Strategy for targeting of vCA1 SST-INs for photoinhibition with halorhodopsin (NpHR) or opsin-negative control vectors (eYFP only) in SST-FlpO mice.

(G) Representative image of viral expression and optic fiber placement (dashed white line). A solid white box indicates the area of magnification (right).

(H) Design for conditioning and extinction of appetitive responding with photoinhibition test at the indicated time point.

(I) Group comparison of entries into the sucrose delivery port as a function of conditioning and extinction.

(J) Effect of SST-IN photoinhibition on sucrose port entries during a 10 min extinction retrieval test, which was divided into 5 min light-on and light-off epochs, analyzed by two-way repeated measures ANOVA. Opsin 3 epoch interaction during extinction retrieval: $F_{(1, 8)} = 19.2$, $p < 0.01$.

(A–E) No Reward: $n = 4$; Reward Ret: $n = 4$; Ext Ret: $n = 4$.

(F–J) eYFP: $n = 5$; NpHR: $n = 5$.

*$p < 0.05$, **$p < 0.01$, ***$p < 0.001$ by Dunn's post hoc test (C), Tukey's post hoc test (E), or Šídák's post hoc test (J). Error bars indicate standard error of mean.

KEY RESOURCES TABLE

REAGENT or RESOURCE	SOURCE	IDENTIFIER
Antibodies		
Rabbit anti-*c*-Fos	Synaptic Systems	Cat#226 003; RRID: AB_2231974
Chicken anti-GFP	Invitrogen	Cat#A11122; RRID: AB_221569
Rabbit anti-somatostatin	Thermo Fischer Scientific	Cat#PA5-82678; RRID: AB_2789834
Goat anti-rabbit Alexa Fluor 647	Jackson ImmunoResearch	Cat#111-605-144; RRID: AB_2338078
Donkey anti-chicken Alexa Fluor 488	Jackson ImmunoResearch	Cat#703-545-155; RRID: AB_2340375
Bacterial and virus strains		
AAV1-Ef1a-fDIO-eYFP	Addgene; Fenno et al. (2014)	Cat#55641 -AAV1; RRID:Addgene_55641
AAV8-nEF-Coff/Fon-ChR2(ET/TC)-eYFP	Addgene; Fenno et al. (2020)	Cat#137141-AAV8; RRID:Addgene_137141
AAV8-nEF-Coff/Fon-NpHR3.3-eYFP	Addgene; Fenno et al. (2020)	Cat#137154-AAV8; RRID:Addgene_137154
AAV8-hSyn-Con/Fon-eYFP	Addgene; Fenno et al. (2014)	Cat#55650-AAV8; RRID:Addgene_55650
AAV8-hSyn-Con/Fon -hChR2(H134R)-eYFP	Addgene; Fenno et al. (2014)	Cat#55645-AAV8; RRID:Addgene_55645
AAV8-Ef1a-fDIO-GCaMP6s	Addgene; unpublished	Cat#105714-AAV8; RRID:Addgene_105714
AAV1-Ef1a-DIO-hChR2(H134R)-eYFP	Addgene; unpublished	Cat#20298-AAV1; RRID:Addgene_20298
AAV8-ESARE-ERCreER-PEST	Boston Children's Hospital Vector Core	N/A
Chemicals, peptides, and recombinant proteins		
4-hydroxytamoxifen (4-OHT)	Sigma-Aldrich	Cat#H6278
Dimethyl sulfoxide (DMSO)	Fischer Scientific	Cat#D1391
ProLong Gold with 4,6-diamidino-2-phenylindole (DAPI)	ThermoFischer	Cat#P36931
Tetrodotoxin citrate (TTX)	Abcam	Cat#ab120055
Experimental models: Organisms/strains		
Mouse: SST-FlpO	Jackson Laboratory	Stock No. 028579; RRID:IMSR_JAX:028579
Mouse: Ai9	Jackson Laboratory	Stock No. 007909; RRID:IMSR_JAX:007909
Mouse: Ai65f	Jackson Laboratory	Stock No. 032864; RRID:IMSR_JAX:032864
Mouse: SST-IRES-Cre	Jackson Laboratory	Stock No. 028864; RRID:IMSR_JAX:028864
Mouse: PV-IRES-Cre	Jackson Laboratory	Stock No. 017320; RRID:IMSR_JAX:017320
Recombinant DNA		
pFBAAV-ESARE-ERCreER-PEST	Gift from Dr. Haruhiko Bito; Kawashima et al. (2013)	N/A
Software and algorithms		
VideoFreeze	Med Associates	https://med-associates.com/product/videofreeze-video-fear-conditioning-software/; RRID:SCR_014574

REAGENT or RESOURCE	SOURCE	IDENTIFIER
Med-PC	Med Associates	https://med-associates.com/product/med-pc/; RRID:SCR_012156
Synapse	Tucker-Davis Technologies	https://www.tdt.com/component/synapse-software/
pMAT	Bruno et al. (2021)	https://github.com/djamesbarker/pMAT; RRID:SCR_022570
Easy Electrophysiology	Easy Electrophysiology	https://www.easyelectrophysiology.com/; RRID:SCR_021190
Any-maze	Stoelting	https://www.any-maze.com/; RRID:SCR_014289
Zen Black	Carl Zeiss	https://www.micro-shop.zeiss.com/en/us/softwarefinder/software-categories/zen-black/; RRID:SCR_013672
FIJI	Schindelin et al. (2012)	https://fiji.sc/; RRID:SCR_002285
pClamp	Molecular Devices	https://www.moleculardevices.com/products/axon-patch-clamp-system/acquisition-and-analysis-software/pclamp-software-suite; RRID:SCR_011323
Prism	GraphPad	https://www.graphpad.com/; RRID:SCR_002798
OriginPro	OriginLab	https://www.originlab.com/; RRID:SCR_014212
SPSS	IBM	https://www.ibm.com/spss; RRID:SCR_002865
BioRender	BioRender	https://www.biorender.com/; RRID:SCR_018361
Illustrator	Adobe	https://www.adobe.com/products/illustrator.html; RRID:SCR_010279